

## SPECTRUM AND ANISOTROPY OF THE COSMIC INFRARED BACKGROUND\*

*J.R. Bond†*

Physics Department, Stanford University;  
Institute for Theoretical Physics, U.C. Santa Barbara

*B.J. Carr*

Astrophysics Group, Fermilab  
Queen Mary College, London University;  
Institute for Theoretical Physics, U.C. Santa Barbara;

*C.J. Hogan*

California Institute of Technology;  
Institute for Theoretical Physics, U.C. Santa Barbara

### ABSTRACT

If the luminosity per mass of the universe at redshifts  $5 \lesssim z \lesssim 1000$  were at least comparable to its present luminosity, then a conspicuous cosmological infrared radiation background would be produced. We survey a number of situations where this could arise and evaluate the intensity of the background for specific types of sources (protogalaxies, pregalactic stars, quasars, black holes, decaying relict particles) in several candidate scenarios, which are also discussed in terms of metal enrichment, dark matter, and formation of large-scale structure. The spectrum of the background radiation is estimated, both with and without dust obscuration. General features of cosmological radiative transfer with dust are discussed. It is argued that dust is expected to degrade the background to the far infrared,  $\approx 100 \mu\text{m}$  to  $1000 \mu\text{m}$ , where the wavelength of the spectral peak can be predicted from the total present day background flux and depends only weakly on properties of the dust or the redshift of emission. We estimate the statistical properties of the anisotropy expected in the radiation and its relationship to the distribution of dust at the time the dust is formed or the radiation is produced. Intensity fluctuations at the few per cent level on arcminute scales are typical. The observability of this anisotropy is evaluated under the assumption that observations will be limited by confusion of foreground extragalactic sources.

---

\*This work was supported by NSF grant AST82-14126 (Caltech) and NASA grant NAGW-299 at Stanford, by the NSF under grant PHY77-27084, supplemented by funds from NASA, the Institute for Theoretical Physics, Santa Barbara, the Theoretical Astrophysics group at Fermilab, and CJH's Bantrell Fellowship.

†Alfred P. Sloan Foundation Fellow

## I. INTRODUCTION

A great gap exists in our direct observations of earlier cosmic epochs, between the highest redshifts  $z \approx 4$  where quasars are observed and the much higher redshift  $z \approx 1000$  where the microwave background is thought to decouple. These "dark ages" were not necessarily devoid of radiation sources; indeed, they are often assumed to include much interesting activity, including the formation of galaxies, the first generation of stars, and the formation of massive black holes which ultimately power quasars. Yet observational searches in the optical and near-infrared for protogalaxies at high redshift have thus far yielded null results. One possible explanation for this non-observation (Sunyaev, Tinsley & Meier 1977) is that young galaxies are shrouded in dusty envelopes which obscure the very energetic activity within. More generally, it could be that any line of sight is likely to encounter an obscuring galaxy at redshifts  $z \gtrsim 4$ , and that this is perhaps the reason why optical and near-infrared searches fail to reveal any sources at higher redshift (see e.g. Ostriker & Heisler 1984.) Pre-galactic radiation from  $z \gtrsim 20$  would be obscured by even a small mean grain abundance, so it is perhaps not surprising that the optical background from these epochs is small.

The place to look for radiation originating in the redshift interval  $5 \lesssim z \lesssim 1000$  is probably in the far-infrared ( $100-1000 \mu\text{m}$ ) for two reasons: (1) energy absorbed by dust is probably re-radiated and redshifted into this band; and (2) the universe is likely to be optically thin at these wavelengths, or at least likely to permit a clear view to much higher redshifts. In this paper we investigate the spectrum and anisotropy of such a cosmological infrared background, the relationship of its observable properties to the composition of the universe and the sources of radiation at various redshifts, and the likelihood of observing such a background with current technology.

Such a study is made more urgent by the rapid progress in far-infrared balloon-borne and satellite telescopes, which for the first time have allowed observations to be made with a sufficient sensitivity to detect a plausible extragalactic background. Let us begin by reviewing the observational situation. To compare bolometric energy flux in very different wavebands, it is useful to express the energy density  $u_\gamma$  in terms of the radiation density per logarithmic or broad-band frequency interval, i.e.  $4\pi\nu I_\nu$ ; to compare with the general cosmological energy budget we express this as a fraction of the closure density ( $\rho_{\text{crit}} = 1.9 \times 10^{-29} h^2 \text{ g cm}^{-3}$  with  $h = H_0/100 \text{ km s}^{-1} \text{ Mpc}^{-1}$ ). This specifies a dimensionless parameter  $\Omega_R$ , which is related to other units by

$$u_\gamma(\lambda) \equiv \lambda \frac{du_\gamma}{d\lambda} \equiv 4\pi\nu I_\nu = 1.1 \times 10^4 \Omega_R h^2 \text{ eV cm}^{-3} = 5.1 \times 10^{-5} \Omega_R h^2 \text{ W cm}^{-2}, \quad (1.1)$$

$$I_\nu = \frac{\Omega_R h^2}{7.4 \times 10^{-7}} \left( \frac{\lambda}{100 \mu} \right) \text{ MJy sr}^{-1}.$$

As a benchmark, the 2.7K background has an integral energy density  $\Omega_{RT} = 2.4 \times 10^{-5} h^{-2}$ , with the spectral energy density (1.1) evaluated at the peak wavelength [ $\lambda_{pk} = (3.9kT/hc)^{-1} = 1400 \mu$ ] giving 74% of this.

Ground based measurements, plagued by atmospheric emission, are not very sensitive to diffuse backgrounds; for example,  $\Omega_R < 3 \times 10^{-5} h^{-2}$  at  $2 \mu\text{m}$  (Hoffman and Lemke 1978). Recently, the tentative detection of a background with  $\Omega_R = 3 \times 10^{-5} h^{-2}$  in the  $2\text{--}5 \mu\text{m}$  band was reported by Matsumoto, Akiba, and Murakami (1984) from a rocket experiment. At somewhat longer wavelengths, better data have been obtained from the IRAS data set. There may be tentative indications of an extragalactic background at  $100 \mu\text{m}$ ; Rowan-Robinson (1985) estimates an extragalactic background of order  $\Omega_R \approx 4 \times 10^{-6} h^{-2}$ , but much of this

is possibly galactic in origin (Low *et al.* 1985, Hauser *et al.* 1984). At longer wavelengths still, Gush (1981) has detected a background at 500-1000  $\mu\text{m}$  from a sounding rocket with  $\Omega_R \approx 10^{-5} h^{-2}$ . This is comparable with upper limits derived from balloon data by de Bernardis *et al.* (1985), whose quoted upper limits at  $\sim 600 \mu\text{m}$  correspond to  $4-7 \times 10^{-6} h^{-2}$  for  $\Omega_R$ . At millimeter wavelengths, spectral distortions in the thermal cosmic microwave background radiation (hereinafter CBR) were reported a few years ago (Woody and Richards 1981) and several authors suggested that partially thermalized pregalactic starlight might explain them (Rowan-Robinson, Negroponte, and Silk 1979; Puget and Heyvaerts 1980; Negroponte, Rowan-Robinson, and Silk 1981; Wright 1982). The distortions are now in doubt (Richards 1984, Peterson *et al.* 1985), but that does not exclude the possibility that the distortions are somewhat weaker or at a somewhat shorter wavelength than first thought. There is considerable scope for improvement in observational techniques, from forthcoming balloon experiments and from the COBE satellite, and this is probably necessary to clarify the observational situation in all of these wavebands.

The following simple argument suggests that a far infrared background, even from high redshift, may be visible above local emission. Suppose that the universe is filled with galaxies having the same intrinsic IR surface brightness and energy spectrum as the local galactic foreground emission, and that this holds true even at high redshift. Consider radiation from the redshift where these galaxies would just cover the sky (this is typically  $1+z \gtrsim 10$ , as shown in §3). The observed integrated surface brightness of a galaxy at redshift  $z$  in an  $\Omega = 1$  universe goes like  $(1+z)^{-4}$  (e.g., Weinberg 1972), so the total brightness of this background will now be a small fraction  $(1+z)^{-4}$  of local galactic brightness. However, the radiation from the high- $z$  galaxies will still be at least comparable with local emission at long wavelengths. This is because the high  $z$  background

peaks at an observed wavelength  $(1+z)$  larger than the local emission, where the latter is smaller than its own peak value by the Rayleigh-Jeans factor  $(1+z)^{-3}$  and by a dust-emissivity factor  $\langle(1+z)^{-1}$  (dust emissivity generally falls off at least as fast as  $\lambda^{-1}$  in the far infrared). The combined effect therefore is that the long wavelength contribution from high- $z$  galaxies is likely to be competitive with local galactic emission. Thus, even very modest extrapolations of present systems to early epochs could produce observable backgrounds at long wavelengths. Similar reasoning applies to radiation which may have been emitted at even higher redshifts, before galaxies formed. It is clear from this argument that one benefits greatly from the spectral effect, which highlights the need for having detectors in the far-infrared.

In section 2, we consider a number of situations where an infrared background might be expected to arise, independently of whether such a background has actually been observed. We calculate the spectrum of the background on the assumption that dust absorption is negligible and we emphasize the connection between the ultimate energy sources in these models and other phenomena, such as the dark matter problem and heavy element production.

Section 3 introduces a simple model for the dust opacity and discusses some simple analytical features of cosmological radiative transfer with dust. The special case of obscuration by familiar types of galaxies is emphasized. Section 4 goes on to discuss the observed reradiated energy spectrum assuming that sources of optical radiation are imbedded in a dust-filled universe. Here we assume that the optical radiation is absorbed by the dust at  $z \gtrsim 5$ , and degraded into a longer wavelength background where the universe is optically thin. It is shown that the observed peak of the emitted radiation spectrum under these conditions depends only very weakly on the redshift or grain properties one may adopt. Quite generally [cf. eq. (4.9)] one obtains a background in the wavelength

band  $\approx 100-1000 \mu\text{m}$ , depending on the total bolometric flux at the present. Ultimately, the insensitivity to the properties of the emitters can be traced to the fact that the flux increases as a high power of temperature. The explicit redshift dependence is weak because a fixed present-day flux implies more optical radiation density, hence hotter grains, as one goes to higher redshift. This key observation will guide much of our detailed discussion.

Sections 5 and 6 apply an equally crude but illustrative model for the anisotropy. There will of course be inhomogeneities both in the amount of dust and in its temperature (e.g. because of its varying proximity to sources of irradiation). Here we estimate anisotropy by assuming that dust is at a uniform temperature but is nonuniformly distributed, which ought to provide a good lower limit to the true anisotropy. The problem then becomes the classic one of background light anisotropy (Shectman 1973, 1974; Peebles 1980), with simplifications from the high-redshift assumption. Observable statistical properties of the background radiation can be related (quite precisely in this simplified model) to the three-dimensional autocorrelation function of the dust. Concrete results are calculated in some representative cases.

In section 7 we regain contact with observation, and compare observable features of the predicted anisotropy with the capability of present and planned instruments, and with expected sources of extragalactic contamination. If such a background is detected, is it realistic to expect to be able to observe its intrinsic anisotropy? The foreground noise for space observations is neither atmospheric emission nor (at long wavelengths and small angular scales at least) zodiacal or galactic emission, but infrared galaxies at  $z \lesssim 1$ . A far-infrared high-redshift background sufficiently intense to appear above local diffuse galactic or zodiacal emission would probably have an anisotropy detectable above the expected contamination from foreground galaxies, particularly with projected

instruments such as SIRTIF. For example, a 1-meter spaceborne telescope could detect fluctuations in a  $300\mu\text{m}$  background generated by emission from dusty protogalaxies at  $z \gtrsim 10$  if they produce a flux  $\Omega_R \gtrsim 10^{-7}$ . Although such statements are necessarily model dependent, the point we wish to emphasize is that the sensitivity of these instruments is such that even a non-observation will place strong constraints on otherwise viable cosmological scenarios. Our conclusions are presented in section 8.

## II. SOURCES OF THE INFRARED BACKGROUND

In this section we discuss several types of high redshift sources which are expected to generate an IR background: primeval galaxies, pregalactic stars (including exploding stars, which may have had profound effects on large scale structure), accreting black holes, and decaying relics of the Big Bang. We will estimate the total radiation density,  $\Omega_{RT}$ , and the peak wavelength,  $\lambda_{pk}$ , of the backgrounds on the assumption that they are unaffected by dust. If this assumption fails, our estimate of  $\Omega_{RT}$  is still applicable but  $\lambda_{pk}$  is modified, as discussed in later sections. The main results of this section are summarized in  $\Omega_{RT}-\lambda_{pk}$  space, Fig. 1a, for various sources; corresponding spectra  $\Omega_R(\lambda)$  are given in Fig. 1b.

### (a) Primeval galaxies

The most plausible source of an IR background would be primeval galaxies, in particular the first generation of galactic stars. Several arguments suggest that there may have been an initial burst of massive star formation in our own galaxy (and presumably others) in order to explain the paucity of low metallicity stars (Truran and Cameron 1971). This implies the existence of a minimal background light density, whose characteristics we now calculate.

The starlight produced by the burst, if received directly, would have a spectrum  $\Omega_R(\lambda)$  peaked at a wavelength

$$\lambda_{pk} \approx 0.6 \left( \frac{1+z_G}{10} \right) \left( \frac{M}{10^2 M_\odot} \right)^{-0.3} \mu\text{m} \quad (10M_\odot < M < 10^2 M_\odot) . \quad (2.1)$$

where  $z_G$  is the redshift of galaxy formation (assumed to be the epoch of the burst) and  $M$  is the characteristic mass of the stars. The  $M$  dependence in Eq. (2.1) reflects the fact that the surface temperature of a star ( $T_S$ ) scales approximately as  $M^{0.3}$  in the range of  $10$ – $10^2 M_\odot$  (Ezer and Cameron 1971); we have normalized the temperature to a value of  $6 \times 10^4 \text{K}$  at  $M = 10^2 M_\odot$  since this is appropriate for Population II metallicity (Bond, Arnett, and Carr 1984). Stars larger than  $10M_\odot$  are expected to produce most of the metals, so we only include them in calculating the minimal background. We also neglect stars with  $M > 10^2 M_\odot$ . For reasonable values of  $M$  and  $z_G$ , one expects  $\lambda_{pk}$  to be in the optical or near IR. If  $\Omega_*$  is the density of the stars in the same units as used for the radiation, the total radiation density is

$$\Omega_{RT} \approx 4 \times 10^{-4} \Omega_* \left( \frac{\varepsilon_R}{0.004} \right) \left( \frac{1+z_G}{10} \right)^{-1} . \quad (2.2)$$

where  $\varepsilon_R$  is the efficiency with which radiation is generated from the rest mass of the stars as a result of nuclear burning: if  $Y \approx 0.25$ ,  $\varepsilon_R = 0.004$  for  $M = 10^2 M_\odot$  (Bond, Arnett, and Carr 1984) and it scales approximately as  $M^{0.5}$  for  $10M_\odot < M < 10^2 M_\odot$  (Iben 1967).

The value of  $\Omega_*$  in Eq. (2.2) is very uncertain but the fact that the burst of star formation has to produce an enrichment  $Z \approx 0.001$  (since this is the prompt initial enrichment required) imposes a *lower limit* on  $\Omega_R$ :

$$\Omega_{RT}(M) > 2 \times 10^{-7} \left( \frac{Z_{ej}}{0.2} \right)^{-1} \left( \frac{\Omega_g}{0.1} \right) \left( \frac{1+z_G}{10} \right)^{-1} \left( \frac{M}{10^2 M_\odot} \right)^{0.5} \left( \frac{Z}{10^{-3}} \right) . \quad (2.3)$$

Here  $\Omega_g$  specifies the gas density of the universe after the burst of star formation and  $Z_{ej}$  is the typical fractional metal yield of the stars. We have normalized  $Z_{ej}$  to 0.2 since this is a reasonable minimum value in the mass range  $10-10^2 M_\odot$ ; however, it could be somewhat higher (up to 0.5) for larger stars (Weaver and Woosley 1980). Since  $M$  is a function of  $\lambda_{pk}$  from Eq. (2.1), we can treat Eq. (2.3) as a "spectral" constraint in  $\Omega_{RT}-\lambda_{pk}$  space (Fig. 1a):

$$\Omega_{RT}(\lambda_{pk}) > 9 \times 10^{-8} \left( \frac{Z_{ej}}{0.2} \right)^{-1} \left( \frac{\Omega_g}{0.1} \right) \left( \frac{1+z_G}{10} \right)^{0.7} \left( \frac{\lambda_{pk}}{\mu} \right)^{-1.7}$$

$$0.6 \left( \frac{1+z_G}{10} \right) < \frac{\lambda_{pk}}{\mu} < 1.2 \left( \frac{1+z_G}{10} \right) \quad (2.4)$$

The form of this constraint is shown by the curve II9 in Fig. 1a, for  $1+z_G = 10$ . In Fig. 1b, the associated spectrum  $\Omega_R(\lambda)$  is plotted assuming that  $30M_\odot$  stars generate the metallicity. The spectrum will be somewhat broader if realistic stellar number densities and galaxy formation redshift ranges are used. (For a black body,  $\Omega_R(\lambda_{pk}) = 0.74\Omega_{RT}$  relates the peak of the spectral density to the integrated radiation density.) Note that a somewhat smaller IR background could be generated by the red supergiant phase of stars above  $10M_\odot$  (Campbell and Terlevich 1984).

One can use the same sort of argument to predict the background associated with the metallicity observed in typical Population I stars ( $Z \sim 0.01$ ). The appropriate redshift is now  $z \leq 1$  if the metallicity was produced recently, so  $\lambda_{pk}$  is decreased and  $\Omega_{RT}$  is increased. Curve I0 in Fig. 1 shows the background associated with an enrichment of  $\Delta Z = 0.01$  at  $z=0$ ; we assume  $\bar{n}_g = 0.1$  although, in this case, a smaller value of  $\Omega_g$  may be more appropriate. Such a background may *have* to be reprocessed by dust in order to avoid the observational constraints in the UV and optical (Peebles and Partridge 1967; Thorstensen and Partridge 1975; Carr, Bond, and Arnett 1984).

There could also be a background from stars smaller than  $10M_{\odot}$  which produce little metal contamination. However, most of these would burn out at  $z < z_G$ : a rough fit for the main-sequence lifetime is  $t_{\text{ms}} \simeq 10^{10}(M/M_{\odot})^{-2.2}$  y for  $1M_{\odot} < M < 10M_{\odot}$  and this exceeds the age of the universe at  $z_G$  unless  $M$  exceeds  $M_* \simeq 5((1+z_G)/10)^{0.7} h^{0.5} \Omega^{0.2} M_{\odot}$ . (The expression for  $M_*$  assumes  $1+z_G > \Omega^{-1}$ .) If we use the approximate relationships  $T_S \propto M^{0.7}$  and  $\varepsilon_R \propto M^{0.3}$  for stars in the range  $M_* > M > 1M_{\odot}$ , we obtain

$$\lambda_{pk} \simeq 0.5 \left( \frac{M}{M_{\odot}} \right)^{0.8} \mu. \quad (2.5)$$

$$\Omega_{RT}(\lambda_{pk}) \simeq 7 \times 10^{-4} \Omega_* \left( \frac{M}{M_{\odot}} \right)^{-1.2} \quad (2.6)$$

$$\simeq 2 \times 10^{-4} \left( \frac{\Omega_*}{0.1} \right) \left( \frac{\lambda_{pk}}{\mu} \right)^{-1.5} \cdot 2 \left( \frac{1+z_G}{10} \right)^{0.5} > \frac{\lambda_{pk}}{\mu} > 0.5.$$

This exceeds the contribution from stars in the range  $10M_{\odot} > M > M_*$ . The redshift of galaxy formation only enters Eq. (2.6) through the long wavelength limit. To show how large  $\Omega_R$  could in principle be from such stars, we plot Eq. (2.6) in curve *IMS* of Fig. 1a for the maximum value (0.1) of  $\Omega_*$  consistent with dynamical constraints.  $\Omega_*$  is likely to be much smaller. Indeed the optical constraints demand that it be much smaller unless the light is reprocessed by grains. Stars smaller than  $1M_{\odot}$  would still be burning: if we assume their luminosity and temperature scale as  $M^4$  and  $M^{0.7}$ , respectively, we obtain

$$\lambda_{pk} \simeq 3 \left( \frac{M}{0.1M_{\odot}} \right)^{-0.7} \mu, \quad \Omega_{RT}(M) \simeq 7 \times 10^{-8} \left( \frac{M}{0.1M_{\odot}} \right)^3 \left( \frac{\Omega_*}{0.1} \right). \quad (2.7)$$

Stars with  $M \leq 0.1M_{\odot}$  could in principle provide the dark matter in galactic halos; curve *LMS* in Fig. 1a shows the associated background if  $M = 0.1M_{\odot}$ .

**(b) Pregalactic stars**

A more speculative source of an IR background would be a population of pregalactic stars. In many cosmological scenarios one would expect such stars to form because the existence of galaxies implies that there must have been density fluctuations in the early Universe, which would in some cases extend at  $z \sim 1000$  down to scales as small as  $\sim 10^6 M_\odot$ . Thus the first objects to form could be pregalactic clouds with this mass (Peebles and Dicke 1968; Carr and Rees 1984; Peebles 1984).

These clouds would presumably fragment into stars. The background radiation generated by these first stars can be derived as in case (a), but the wavelengths will be reduced by about 0.6 (because zero-metallicity stars are somewhat hotter than Population II stars) and the appropriate values of  $\Omega_*$ ,  $M$ , and  $z$  will be different. The value of  $M$  is particularly uncertain. Some authors have argued that the first stars could be much smaller than today ( $M < 0.1 M_\odot$ ) due to molecular cooling (e.g. Palla, Salpeter, and Stahler 1984). In this case, most of the light would be produced at the present epoch ( $z \sim 1$ ) and the fact that the stars were pregalactic would be largely irrelevant. Others have argued that the first stars could be much more massive than the ones forming today (perhaps in the VMO range above  $10^2 M_\odot$ ) due to the lack of metallicity and/or the effects of the 3K background (e.g., Silk 1977, Terlevich 1983, Kashlinsky and Rees 1983). Pregalactic clouds might collapse and the first stars form at a redshift  $z_F$  around 100; providing

$$z_F < z_{ms}(M) \simeq 300 \min \left[ 1, \left[ \frac{M}{10^2 M_\odot} \right] \right] (\Omega h^2)^{-1/3} \quad (M > 10 M_\odot), \quad (2.8)$$

this is also the redshift at which most of the light from stars of mass  $M$  will be produced. Therefore  $z_* = \min(300, z_F)$  is the redshift of light production.

The value of  $\Omega_*$  cannot be predicted in the pregalactic star model, but it can be constrained (Carr, Bond, and Arnett 1984). For example, if we assume that the pregalactic enrichment cannot exceed  $10^{-3}$  (the minimum metallicity observed in Population I stars), this implies a limit on the density of radiation from stars in the mass range  $z_*/3 < M/M_\odot < 10^2$  of the form given by Eq. (2.3) with  $z_G \rightarrow z_* \simeq 100-300$ . Since  $\lambda_{pk}$  is 0.6 times the value of Eq. (2.1), this gives

$$\Omega_{RT}(\lambda_{pk}) < 2 \times 10^{-7} \left( \frac{Z_{ej}}{0.2} \right)^{-1} \left( \frac{\Omega_g}{0.1} \right) \left( \frac{1+z_*}{100} \right)^{0.7} \left( \frac{\lambda_{pk}}{\mu} \right)^{-1.7}$$

$$4 \left( \frac{1+z_*}{100} \right) < \frac{\lambda_{pk}}{\mu} < 5 \left( \frac{1+z_*}{100} \right)^{0.7} \quad (2.9)$$

For stars in the range  $10 < M/M_\odot < z_*/3$ , which burn out after  $z_*$ , Eq. (2.8) implies

$$\lambda_{pk} = 2 \left( \frac{M}{10M_\odot} \right)^{0.7} \mu.$$

$$\Omega_{RT}(\lambda_{pk}) < 4 \times 10^{-8} \left( \frac{\lambda}{\mu m} \right)^{-0.7} \left( \frac{Z_{ej}}{0.2} \right)^{-1} \left( \frac{\Omega_g}{0.1} \right), \quad 5 \left( \frac{1+z_*}{100} \right)^{0.7} > \frac{\lambda_{pk}}{\mu} > 2. \quad (2.10)$$

(These limits are very conservative; it might be more reasonable to assume that the pregalactic enrichment cannot exceed  $10^{-5}$ , corresponding to the minimum Population II metallicity (Bond 1981), in which case  $\Omega_{RT}$  is reduced by 100.) Curve //100 in Figs. 1a,b indicates the maximum background consistent with Eqs. (2.9) and (2.10). Since  $z_* < 300$ , the peak of the undegraded background never appears beyond  $12 \mu$ .

If the stars were in the mass range  $200-10^5 M_\odot$ , they would be expected to collapse to black holes after their main-sequence phase without any metal ejection (Bond, Arnett, and Carr 1984). Here our best constraint is that these holes should eventually cluster inside galaxies, so the density of their precursors must

satisfy  $\Omega_* < 0.1$  in order to avoid making too much dark matter in galactic halos (Faber and Gallagher 1979). From Eq. (2.2), one thus has a limit for their pre-black hole radiation

$$\Omega_{RT}(\lambda_{pk}) < 4 \times 10^{-8} \left( \frac{1+z_*}{100} \right)^{-1} \left( \frac{\Omega_*}{0.1} \right), \quad \lambda_{pk} \simeq 4 \left( \frac{1+z_*}{100} \right) \mu \quad (2.11)$$

where we use the fact that  $\varepsilon_R$  and  $T_S$  are independent of  $M$  for such stars. Of course, if VMOs with  $M > 200M_\odot$  formed efficiently, their remnants might be good candidates for explaining the dark matter (Carr, Bond, and Arnett 1984). Black holes could also derive from SMOs (i.e., stars larger than  $10^5M_\odot$ ) since these may collapse directly, even before burning their nuclear fuel, as a result of relativistic instabilities (Fowler 1966; Fricke 1973). However, black holes larger than  $10^6M_\odot$  are precluded from providing galactic halos by dynamical constraints (Carr 1977; Lacey 1984), so there is only a narrow mass range in which pregalactic stars could generate the dark matter without also generating considerable radiation. The maximum IR background from pregalactic VMOs with  $M > 200M_\odot$  is shown by curve *VMO* in Figs. 1a,b. Clearly, if the dark matter does derive from such stars, the existence of a large IR background is an inevitable consequence: Eq. (2.11) with  $z_* \simeq 10$  implies that  $\Omega_R$  could be as high as  $4 \times 10^{-5}$ .

### (c) Black holes

A third source of an IR background could be accreting black holes, such as the precursors of the black holes which are currently thought to power quasars (e.g. Rees 1978) or holes hypothesized to explain the dark matter in halos. A great deal of uncertainty exists because the luminosity of the holes depends on how they are fueled, and how the energy released in accretion is reprocessed in the surrounding medium before escaping.

If  $\Omega_{b,acc}$  is the mass density of the matter which accreted onto the holes at redshift  $z_*$  and  $\varepsilon$  is the efficiency of its conversion to radiation, then

$$\Omega_{RT} = \varepsilon \Omega_{b,acc} (1+z_*)^{-1}. \quad (2.12)$$

Clearly, a large abundance of efficiently accreting holes can be strongly ruled out from background light constraints. We consider two models: one in which  $\Omega_{b,acc} \sim \Omega_b$  and which might be applicable to active galactic nuclei (hereinafter, AGN's), and the other in which  $\Omega_{b,acc} \ll \Omega_b$  and is perhaps more appropriate to smaller black holes accreting in the pregalactic medium.

First consider a case which might apply to observed galactic nuclei (see e.g. Begelman, Blandford, and Rees 1984). Assume that each present-day galaxy contains a  $10^8 M_\odot$  hole, and that at  $z_* \simeq 10$  each of these holes radiated at the Eddington limit  $\dot{M}_E$  for the time it takes to double its mass. (This applies, in particular, if the hole derived from a much smaller initial "seed" hole.) This timescale is the mass-independent "Salpeter time"

$$(\dot{M}_E / M)^{-1} = 4.1 \times 10^8 \varepsilon \text{ y} \quad (2.13)$$

which equals the age of the universe at  $1+z = 6.4 \Omega^{-1/3} h^{-2/3} \varepsilon^{-2/3}$ . With  $\Omega \simeq 0.1$  in galaxies and  $10^{12} M_\odot$  per galaxy,  $\Omega_{b,acc} \simeq 10^{-5}$ , hence  $\Omega_{RT} \simeq 10^{-6} \varepsilon ((1+z_*)/10)^{-1}$ . Much of the bolometric luminosity in such an Eddington-limited flow is thought to come from the photosphere of an optically thick accretion torus and to produce a roughly thermal spectrum with temperature  $\sim 20 - 30,000$  K (Begelman 1984), corresponding to an observed peak wavelength  $\lambda_{pk} \sim 2\mu[(1+z_*)/10]$ . More generally, if blackbody emission occurs from a photosphere at a distance  $10\xi_1 GM/c^2$  from a hole of mass  $M \equiv 10^8 M_\odot$ , where  $\xi_1 \sim 1$  would correspond to the inner edge of an accretion disk, then the temperature would be

$$T = 5.5 \times 10^5 K \xi_1^{-1/2} (\dot{M} / \dot{M}_E)^{1/4} M_6^{-1/4} . \quad (2.14)$$

The low temperatures observed in AGN's seem to imply large  $\xi_1$ , and hence large, optically thick accretion tori.

However, this picture may be inappropriate for pregalactic holes. For the case of halo holes accreting from a nearly uniform medium in their early history,  $\dot{M}$  may be much less than the Eddington rate. To estimate  $\Omega_R$  we adopt the Bondi (1952) accretion rate for  $\dot{M}$  appropriate to spherically symmetric accretion onto slowly-moving holes located in a medium with gas density  $n_g$  and temperature  $T = 10^4 T_4 K$ :

$$\dot{M}_B / M = (5.3 \times 10^8 y)^{-1} M_6 (n_g / \text{cm}^{-3}) T_4^{-3/2} . \quad (2.15)$$

We parametrize the gas density by  $n_g = 1.1 \times 10^{-5} \Omega_g \delta h^2 (1+z)^3 \text{cm}^{-3}$ , where  $\delta$ , the gas clumpiness relative to the cosmological average, could be quite large. The fraction of material accreted over a Hubble time at redshift  $z_*$  is relatively small (unless  $\delta$  is large), yielding an associated radiation density

$$\Omega_{RT} \simeq 6.6 \times 10^{-6} \left( \frac{\varepsilon}{0.1} \right) M_6 \left( \frac{\Omega_b}{0.1} \right) \Omega_g \delta h \Omega^{-1/2} T_4^{-3/2} \left( \frac{1+z_*}{10} \right)^{1/2} \quad (2.16)$$

(Carr, McDowell, and Sato 1983). Though  $\varepsilon$  may be quite small if accretion is truly spherically symmetric, the Bondi formula still applies for gas with sufficient angular momentum to form a disk, since the accretion radius is  $R_A \sim 5 \times 10^8 T_4^{-1} GM / c^2$ ;  $\varepsilon \sim 0.1$  is plausible for thin disks.

Radiation from thin disks may be predominantly nonthermal, though a blackbody could arise for sufficiently small accretion rates,  $\dot{M} / \dot{M}_E < 1.2 \times 10^{-2} \varepsilon M_6^{-1/8}$  (Eardley *et al.* 1978). The temperature is approximately given by Eq. (2.14) with  $\xi_1 \sim 1$  (cf. Begelman 1984). With  $\dot{M}$  given by Eq. (2.15), we have

$$T_{disk} \approx 3 \times 10^4 K \left( \frac{\varepsilon}{0.1} \right)^{1/4} \left( \frac{\Omega_g \delta h^2}{0.1} \right)^{1/4} T_4^{-3/8} \xi_1^{-1/2} \left( \frac{1+z_*}{10} \right)^{3/4} . \quad (2.17)$$

hence an observed peak wavelength

$$\lambda_{pk} \approx 1.3 \mu \left( \frac{\varepsilon}{0.1} \right)^{-1/4} \left( \frac{\Omega_g \delta h^2}{0.1} \right)^{-1/4} T_4^{3/8} \xi_1^{1/2} \left( \frac{1+z_*}{10} \right)^{1/4} . \quad (2.18)$$

The background level expected for Bondi accretion with  $\delta \sim 1$  at  $z_* = 40$  for a dark matter density ( $\Omega_b \sim 0.1$ ) of  $10^6 M_\odot$  holes is indicated by curve VMBH in Fig. 1a. The value  $z_* = 40$  is chosen because Carr et al. (1983) argue that this is the redshift at which the Bondi rate first satisfies the Eardley et al. criterion for a thermal spectrum and most of the radiation should come from that epoch.

If  $\delta$  or  $z_*$  is large enough,  $\dot{M}_B$  can exceed  $\dot{M}_E$  and accretion would be Eddington-limited. This could conceivably apply even for the dark matter holes, in which case Eq.(2.12) implies a very high value of  $\Omega_{RT}$  indeed. It should anyway apply for black holes in active galactic nuclei: curve AGN9 in Fig.1 indicates the background from Eddington-limited accretion at  $z_* = 9$  with  $\Omega_b \sim 10^{-5}$ .

**(d) Formation of large scale structure**

Several authors have proposed that galaxy clustering is a byproduct of energetic events at high redshift. In a scenario proposed by Ostriker and Cowie (1981), the structure is created by hydrodynamic motions of gas caused by supernova explosions. The thermal energy density required to generate structure having  $(\delta\rho/\rho) \sim 1$  on a comoving scale  $d = 10d_{10}Mpc$  is characteristically of order (Hogan 1984)

$$\rho_{thermal} c^2 \simeq m_N (H(z_x) d (1+z_x)^{-1})^2 n_b \simeq 10^{-2} eV \text{ cm}^{-3} (1+\Omega z_x) (1+z_x)^3 \left( \frac{\Omega_g h^2}{0.1} \right) (hd_{10})^2 \quad (2.19)$$

where  $m_N$  is the nuclear mass,  $\Omega_g$  is the density parameter of gas destined to form clustered galaxies, and  $z_x$  is the epoch of the explosions. Suppose supernovae generate  $100\varepsilon_2$  times as much energy in optical light, including all of the light radiated by their main sequence progenitors (which probably exceeds the light from the blast itself), as they do in blast energy. Then their radiation background would have an energy density (for  $\Omega = 1$ ) independent of  $z_x$ :

$$\Omega_{RT} \simeq 10^{-4} \varepsilon_2 \Omega_{g,-1} h^2 d_{10}^2 . \quad (2.20)$$

Sample parameters for supernovae explosions are  $\varepsilon_2 \sim 0.3$  for  $10M_\odot$  stars and  $\sim 3$  for  $50M_\odot$  stars. However, a metallicity constraint applies to the explosive energy available from metal producing supernovae: with optimal parameters,

$$\rho_{exp} c^2 \lesssim 2 \times 10^{-3} eV \text{ cm}^{-3} (\Omega_g h^2 / 0.1) (1+z_*)^3 (Z / 10^{-2}) , \quad (2.21)$$

where  $Z$  is the allowed average metallicity. This limits the characteristic scale  $d$  over which nonlinear structure may arise. It is also possible to have explosions which eject no metals, involving VMOs (Bond, Arnett, and Carr 1984) or the jet energy from AGNs.

These estimates obviously depend somewhat on the details of how the explosive energy release translates into nonlinear structure for motion, but any similar scheme is likely to produce an intense background.

A different mechanism (Hogan 1983; Hogan and Kaiser 1983) is to generate large-scale structure using radiation-pressure gradients from pregalactic radiation sources at  $z \gtrsim 100$ . This mechanism can be much more energy-efficient than the previous one. Even so, successful and plausible models of this type usually require an infrared flux  $\gtrsim 1\%$  of the microwave background flux, or  $\Omega_R \gtrsim 10^{-7}$ . So it appears that if galaxy clustering energy is not a primordial phenomenon, the concomitant waste heat from whatever process produced it is likely to be observable.

#### (e) Decaying Particle Backgrounds

Decaying weakly interacting relics of the Big Bang which have photons in one of their decay channels generate an electromagnetic background. The amplitude and wavelength regime depend upon the abundance parameter  $\Omega_X$  the massive relic particles (which we call  $X$ ) would have had today had they not decayed, their mass,  $m_X$ , their lifetime  $\tau_X$  (or, equivalently, their decay redshift  $z_d$  defined by  $H(z_d)\tau_X = 1$ ), and their branching ratio to the photon decay modes,  $B_X$ . For heavy neutrinos of mass  $< 1 MeV$ , Silk and Stebbins (1983) have shown that, if  $\tau_X < 50 y$ , the decay energy is unobservable, being predominantly redistributed into the microwave background. If  $50y < \tau_X < 3 \times 10^4 y$ , the decay energy will give a Bose-Einstein distortion of the CBR with a nonzero chemical potential which current observations now strongly constrain. Longer lifetimes give backgrounds with present spectra which just reflect the redshift of the photon decay energy.

For illustration, consider nonrelativistic relics decaying in the epoch after Bose-Einsteinization. Corrections for relativistic decay are straightforward (Silk and Stebbins 1983) and do not affect the result appreciably in the regime of interest to us. We assume a radiative decay mode  $X_H \rightarrow X_L + \gamma$  where the weakly interacting product  $X_L$  is taken to be much lighter than  $X_H$ : the photons are then produced with an energy  $m_X/2$ . When redshift effects are taken into account, the energy now at the peak of the spectrum is  $C_\lambda m_X/(1+z_d)$ , where  $C_\lambda \approx 1$  is a constant which depends upon whether  $z_d$  falls in the radiation or matter dominated era. The peak wavelength now is

$$\lambda_{pk} \approx \frac{124\mu}{C_\lambda} \left[ \frac{1+z_d}{10^5} \right] (m_X/keV)^{-1}. \quad (2.22)$$

The density in decay radiation is

$$\Omega_{RT} = \frac{1}{2} C_E \frac{B_X \Omega_X}{1+z_d} = 5 \times 10^{-6} C_E B_X \Omega_X \left[ \frac{10^5}{1+z_d} \right] \quad (2.23)$$

where  $C_E \approx 1$  is another constant depending upon the epoch of decay. Thus a  $1keV$  particle decaying at redshift  $10^5$  with abundance  $\Omega_X \sim 1$  and  $B_X \sim 1$  would produce a  $100\mu$  background at the  $5 \times 10^{-6}$  level, near the limit of IRAS sensitivity.

We have assumed that there is no relationship between  $\Omega_X$ ,  $m_X$ ,  $\tau_X$ , and  $B_X$ . For specific models, there will be. For example, for massive neutrinos with  $m_\nu < 1MeV$ ,  $\Omega_\nu h^2 = 10(m_\nu/keV)$ :  $1keV$  neutrinos decaying at  $z \sim 10^5$  could then be ruled out by current IRAS limits (Low *et al.* 1985; Rowan-Robinson 1985) if  $B_\nu \sim 1$ . Typical neutrino decay models give lifetimes much longer than this (de Rujula and Glashow 1980).

The spectral shape is typically of form

$$\Omega_R(\lambda) \propto (\lambda_{pk}/\lambda)^p \exp\{-2C_s(\lambda_{pk}/\lambda)^p\}. \quad (2.24)$$

where the constant  $C_S \approx 1$  and the power  $p$  is 1.5 or 2 depending upon whether  $z_d$  lies in the matter or radiation dominated eras. The spectrum is plotted in Fig. 1b (curve DP) for a particle with  $B_X \Omega_X = 10^{-2}$  decaying with a lifetime  $6 \times 10^5 y$  ( $z_d = 10^3$ ) in an  $\Omega = 1$ ,  $h = 0.5$  universe.

### III. THE OPACITY DUE TO DUST GRAINS

In this section we will examine how the presence of dust can modify the spectra derived in Sec. 2. By making rather simplistic assumptions about the form of the grains, we derive the radiative transfer equation and use this to determine the circumstances in which the Universe goes opaque.

#### (a) Grain characteristics

Let us assume that a fraction  $\Omega_d$  of the critical density is in the form of grains. The absorption cross-section of each grain is close to its geometric cross-section for wavelengths  $\lambda$  well below the grain size  $\tau_d$ , but for typical grains it falls off roughly as  $\lambda^{-1}$  for wavelengths between  $\tau_d$  and  $200\mu$ ; at longer wavelengths the slope steepens, tending to  $\lambda^{-2}$  at around  $10^3\mu$  (Erickson *et al.* 1981; Schwartz 1982; Draine and Lee 1984). For simplicity, we assume the grains are spherical. Unless they are extremely elongated, and are also good conductors, these assumptions will not change our results by more than a factor of order unity (Purcell 1969; Hildebrand 1983; Wright 1982). Many of our results carry over to the case of molecular opacity (see Appendix).

Since we are generally interested in absorption in the optical and UV, and emission in the IR, a convenient expression for the grain absorption rate at frequency  $\omega$  is

$$\Gamma_d(\omega, \mathbf{x}, t) = n_d(\mathbf{x}, t) \sigma_d c \left[ 1 + \left( \frac{\omega_d}{\omega} \right)^a \right]^{-1} \quad (3.1)$$

Here  $\sigma_d = \pi r_d^2$ ,  $n_d$  is the grain number density at position  $\mathbf{x}$  and time  $t$ , and  $\omega_d = c C_d / r_d$  is an angular frequency characterizing the onset of the  $\lambda^{-1}$  behavior. (Typically  $C_d \simeq 1$ , so the equivalent wavelength is  $\lambda_d = 2\pi r_d$ .) The value of  $r$  is known to vary widely for grains in the galaxy; models typically have a spectrum of sizes between  $0.01\mu$  and  $0.3\mu$  (Mathis, Rumpl and Nordsieck 1977). An intermediate value of  $0.1\mu$  is here adopted as a fiducial standard. Equation (3.1) ignores all resonant effects; spectral features with  $\delta\lambda/\lambda < O(1)$  would be important for observations with good spatial and spectral resolution (Hogan and Rees 1979) but can be neglected for many purposes because they tend to be smeared out by cosmological redshift effects into an effective continuum (see Appendix). We are also ignoring scattering processes: although these have a cross-section comparable to that for absorption if  $\omega \geq \omega_d$ , they are irrelevant for our purposes.

**(b) The radiative transfer equation with dust**

The effect of the dust on the background radiation can be derived by considering the radiative transfer equation. If we neglect scattering, Doppler shifts, stimulated emission, and polarization, the transfer equation for the distribution function  $f(q, \mathbf{x}, t)$  in an expanding Universe takes the form:

$$\left. \frac{\partial f}{\partial t} \right|_{\mathbf{q}} + \frac{1}{a} \hat{\mathbf{q}} \cdot \nabla f = \Gamma_a(\mathbf{q}, \mathbf{x}, t)(f_{eq} - f) + P_S(\mathbf{q}) \quad (3.2)$$

where

$$f_{eq} = \left[ \exp \left( \frac{q}{a T_d} \right) - 1 \right]^{-1}. \quad (3.3)$$

The general relativistic scalar  $f$  is the mean occupation number of the comoving momentum state  $\mathbf{q}$  in the neighborhood of the spacetime point  $(\mathbf{x}, t)$ ,  $f_{eq}$  is

the Planck distribution function,  $P_S$  is the radiant emission incident upon the grains, and  $a = (1+z)^{-1}$  is the cosmological scale factor. The grains are assumed to be in thermal equilibrium internally with temperature  $T_d$ . We take  $\hbar = c = k = 1$ , so the photon energy is an angular frequency  $\omega$  and the temperature is in energy units. The angular frequency observed at the present epoch is  $q = \omega a$  and the associated wavelength is  $\lambda = 2\pi/q$ . In this section and the next we consider only the angle-averaged version of Eq. (3.2) for spatially uniform  $T_d$ . The spatial gradients and  $x$ -dependence of the absorption rate are therefore ignored, although they are explicitly taken into account in Secs. 5 and 6.

The emission rate of the grains into the momentum space volume  $d^3q / (2\pi a)^3$  is  $\Gamma_a f_{eq}$ . This is related to the grain luminosity density for radiation in the frequency band  $(\omega, \omega + d\omega)$ ,  $\mathcal{L}_d(\omega, t) d\omega / \omega$ , by

$$\mathcal{L}_d(\omega, t) = \frac{1}{\pi^2} \left( \frac{q}{a} \right)^4 \Gamma_a(q, t) f_{eq}(q, t). \quad (3.4)$$

Similarly, the luminosity density  $\mathcal{L}_S(\omega, t)$  associated with the source term  $P_S$  in Eq. (3.2) is

$$\mathcal{L}_S(\omega, t) = \frac{1}{\pi^2} \left( \frac{q}{a} \right)^4 P_S(q, t). \quad (3.5)$$

For sources which emit before the dust is formed, the time-integration of  $P_S(q)$  just gives rise to the distribution function  $f(q, t_S)$  at some initial time  $t_S$ . If thermal sources are homogeneous, we then get

$$f_S(q, t) = \int_{t_S}^t dt' n_S(t') L(t') \frac{15}{\pi^2 T_S^4} \left[ \exp \left( \frac{q}{a(t') T_S} \right) - 1 \right]^{-1}. \quad (3.6)$$

Here  $L$ ,  $T_S$  and  $n_S$  are the luminosity, temperature, and number density of the sources. Added to this is the thermal CBR distribution function.

(c) The angle-averaged optical depth

If we neglect spatial gradients and re-emission, the homogeneous transfer equation has the simple solution

$$f(q,t) = f(q,t_S) \exp[-\bar{\tau}(q,t_S) + \bar{\tau}(q,t)]. \quad (3.7)$$

Here  $\bar{\tau}(q,t)$  is the angle-averaged optical depth of the Universe for a photon of present momentum  $q$  from the present ( $t_0$ ) back to time  $t$ :

$$\bar{\tau}(q,t) = \int_t^{t_0} \Gamma_a(t) dt = \left[ \frac{n_d(t) \sigma_d c t}{1 + \left(1 + \frac{2\alpha}{3}\right) \left(\frac{a\omega_d}{q}\right)^\alpha} \right]_t^{t_0}. \quad (3.8)$$

(The form of the denominator comes from evaluating the integral in the high and low frequency limits and linearly interpolating.) In terms of the reduced observed wavelength  $\lambda \equiv \lambda / 2\pi = q^{-1}$  and the redshift  $z$ , we have

$$\begin{aligned} \bar{\tau}(\lambda, z) &= \frac{1}{2} \Omega_d \Omega^{-1/2} \rho_{\text{crit}} \rho_{\text{id}}^{-1} c H_0^{-1} r_d^{-1} (1+z)^{3/2} \left[ 1 + \frac{5}{3(1-\varepsilon)} \left( \frac{\lambda \alpha}{r_d} \right)^\alpha \right]^{-1} \\ &\simeq 1.3 \Omega_{d,-5} \Omega^{-1/2} h (2 / \rho_{\text{id}}) (0.1 \mu / r_d) \left( \frac{1+z}{10} \right)^{3/2} \left[ 1 + \frac{5}{3(1-\varepsilon)} \left( \frac{\lambda \alpha}{r_d} \right)^\alpha \right]^{-1}. \end{aligned} \quad (3.9)$$

$$\varepsilon = \frac{2(\alpha-1)}{3+2\alpha},$$

where we used the relation  $t = \frac{2}{3} H_0^{-1} \Omega^{-1/2} (1+z)^{-3/2}$ , which is valid for  $1+z > \Omega^{-1}$ ;  $H_0^{-1} \simeq 3 \times 10^{17} h^{-1} \text{s}$  is the Hubble time and  $\rho_{\text{id}}$  is the internal grain density in  $\text{g cm}^{-3}$ . The redshift at which  $\bar{\tau}$  reaches 1 is thus given by

$$\begin{aligned} 1+z_1 &= 10 \left( \frac{\lambda}{\mu} \right)^{2/5} \left[ 1.1 \Omega_{d,-5}^{-2/5} \Omega^{1/5} h^{-2/5} \left( \frac{\rho_{\text{id}}}{2} \right)^{2/5} (1-\varepsilon)^{-2/5} \right]^{(1-\varepsilon)} \\ &\times \left( \frac{r_d}{0.1 \mu} \right)^{-\varepsilon} \left( \frac{\lambda}{\mu} \right)^{3\varepsilon/5}, \quad \lambda > r_d / \alpha \end{aligned} \quad (3.10a)$$

$$= 8.2\Omega_{d,-5}^{-2/3}\Omega^{1/3}h^{-2/3}\left(\frac{\tau_d}{0.1\mu}\right)^{2/3}(\rho_{id}/2)^{2/3}, \quad \lambda < \tau_d/a, \quad (3.10b)$$

where  $\Omega_{d,-5} \equiv 10^5 \Omega_d$ . The form of (3.10) is relatively simple if  $\alpha = 1$  ( $\varepsilon = 0$ ). Fig. 2 indicates the  $\lambda$ -dependence of this redshift for a particular case.

In the  $\lambda > \tau_d(1+z)$  case, it will also be useful to express the critical redshift for absorption in terms of the emitted wavelength [ $\lambda_e = \lambda(1+z)^{-1}$ ]:

$$1+z \simeq 12\left(\frac{\lambda_e}{0.1\mu}\right)^{2/3}[\Omega_{d,-5}\Omega^{-1/2}(\rho_{id}/2)^{-1}h(1-\varepsilon)^{-1}]^{-2/3}\left(\frac{\lambda_e}{\tau_d}\right)^{2(\alpha-1)/3}, \quad \lambda_e > \tau_d. \quad (3.11)$$

This equation specifies the minimum grain abundance required to make the Universe opaque to radiation of given emitted wavelength at a redshift  $z$ . In the  $\lambda < \tau_d(1+z)$  case, the equivalent condition can be derived directly from Eq. (3.10b). The opaque  $(\Omega_d, z)$  regime in this case is indicated in Fig. 3.

So far we have assumed that the grain abundance is fixed. However,  $\Omega_d$  must itself be a function of  $z$ , so Eq. (3.10) only determines the redshift when the Universe goes opaque implicitly. One can regard  $\Omega_d(z)$  as specifying a trajectory in Fig. 3. The Universe will be optically thick to dust absorption for some period providing this trajectory penetrates the opaque region. Note, however, that Fig. 3 assumes  $\lambda < \tau_d(1+z)$  and absorption is only guaranteed for radiation which always satisfies this condition. If the radiation is generated before the grains, it may be redshifted to the waveband in which the absorption efficiency is reduced before it encounters them. Thus penetration of the opaque region in Fig. 3 is a necessary but not sufficient condition for absorption. Whether or not  $\Omega_d(z)$  does penetrate the opaque region is uncertain. Since quasar-reddening measurements imply that a *uniform* dust distribution must have  $\Omega_d < 6 \times 10^{-5} h^{-1}$  for  $z < 2$  (Wright 1981),  $\bar{\tau}$  is certainly below 1 at the present epoch. On the other hand, this limit does not apply for clumpy dust (Ostriker and Heisler 1984) and

in any case only a tiny abundance would be required to ensure absorption at high redshifts. For example, Matsumoto *et al.*'s (1983) IR background (if real) might derive from unabsorbed pregalactic stars at  $z = 100$  (Carr, McDowell, & Sato 1983), but even an  $\Omega_d$  of  $10^{-6}$  at such a redshift would suffice to absorb the starlight (de Bernardis *et al.* 1985).

**(d) Absorption by dust in galaxies**

As emphasized by Ostriker and Heisler (1984) and Alfvén and Mendis (1977; but see Pollaine 1978), it is possible that the dust in galaxies alone could provide sufficient opacity to absorb any pregalactic background. The contribution of galactic dust to  $\Omega_d$  can be written as

$$\Omega_d = 10^{-5} \left( \frac{\varphi_d}{0.01} \right) \left( \frac{\varphi_g}{0.1} \right) \left( \frac{\Omega_{GB}}{0.01} \right) \quad (3.12)$$

where  $\varphi_d$  is the fraction of the gas mass in dust,  $\varphi_g$  is the fraction of the galactic baryons in gaseous form, and  $\Omega_{GB}$  is the density parameter associated with the baryons in galaxies. Thus,  $\Omega_d \sim 10^{-5}$  is a typical galactic contribution, and  $\Omega_d \approx 10^{-4}$  is feasible at early times if some dust is later swallowed by stars.

Provided the redshift of galaxy formation exceeds the redshift at which  $\bar{\tau} = 1$ , given by Eq. (3.10b), pregalactic radiation will, on the average, be absorbed by intervening dust in galaxies. However, if the dust is sufficiently clumped that it does not cover the sky, then most pregalactic photons could propagate to the observer unimpeded even though the average value of  $\bar{\tau}$  exceeds 1. Thus, in order to ensure absorption, we must supplement Eq. (3.10b) with the covering condition. If the galaxies have a radius  $R_G = 10R_{G10} \text{ kpc}$  and comoving number density  $n_{G*}$  (assumed constant), then their covering factor at redshift  $z$  (i.e., the fraction of sky covered if this is less than 1 or the number of galaxies along a typical line of sight if this exceeds 1) is

$$K = \bar{N}_G(z) \simeq n_{G*} \pi R_G^2 c t_0 \Omega^{-1/2} [(1+z)^{3/2} - 1], \quad (1+z > \Omega^{-1}). \quad (3.13)$$

This reaches 1 at a redshift

$$1 + z_{\text{cov}} = 11 R_{G10}^{2/3} \left( \frac{\rho_{iGB}}{10^{-24} \text{ g cm}^{-3}} \right)^{2/3} \left( \frac{\Omega_{GB}}{0.01} \right)^{-2/3} (\Omega h^{-1})^{1/3}, \quad (3.14)$$

comparable to the redshift (3.10b) at which  $\bar{\tau}$  reaches 1. The galaxies have been assumed to have a uniform internal density in baryons,  $\rho_{iGB}$ , and baryonic mass  $M_{GB} = 4\pi\rho_{iGB}R_G^3/3$ . The density parameter for baryons in galaxies is then given by

$$\Omega_{GB} = 2 \times 10^{-3} \left( \frac{n_{G*}}{0.01 h^3 \text{ Mpc}^{-3}} \right) \left( \frac{\rho_{iGB}}{10^{-24} \text{ g cm}^{-3}} \right) R_{G10}^3 h, \quad (3.15)$$

where the normalization of  $n_{G*}$  is that of bright galaxies. Dwarf galaxies, especially at early epochs, would give much larger values of  $n_{G*}$ .

Note that the covering factor is just the optical depth given by Eq. (3.9) divided by the optical depth associated with an individual galaxy; for wavelengths less than  $\tau_d$ , the latter is

$$\Delta\tau = \bar{\tau} / \bar{N}_G = \left( \frac{R_G}{\tau_d} \right) \left( \frac{\rho_{iGB}}{\rho_{id}} \right) \varphi_d \varphi_g \simeq 1.5 \left( \frac{\varphi_d \varphi_g}{10^{-3}} \right) \left( \frac{\tau_d}{0.1 \mu} \right)^{-1} \left( \frac{\rho_{iGB}}{10^{-24} \text{ g cm}^{-3}} \right) R_{G10} \left( \frac{2}{\rho_{id}} \right) \quad (3.16)$$

A more precise treatment of the effect of galactic obscuration would obviously have to allow for the way in which the grain abundance in the protogalaxy builds up as its radius decreases. At present a typical galaxy has  $\Delta\tau \lesssim 1$  (although it may be opaque along some lines of sight if it forms a disk). However, both the factors  $\varphi_d$  and  $\varphi_g$  change with time, so a typical galaxy could still pass through a phase in which  $\Delta\tau$  exceeds 1. Initially the galaxy will contain no grains and so any starlight will propagate out unimpeded. After a while, however,  $\varphi_d$  may reach a value at which the light gets absorbed before escaping

from the galaxy ( $\Delta\tau > 1$  in Eq. (3.16)). This is certainly plausible if  $\varphi_g$  remains of order unity during the dust build-up. Eventually, as continued star formation decreases the gas content, the galaxy may become optically thin again. It is not inevitable that galaxies pass through an optically thick period like this, but if they do, it would have important consequences for quasar evolution. It would also invalidate some of the considerations of the next two sections. IRAS results seem to indicate that only a small fraction of galaxies at the present absorb most of their own optical emission (Soifer *et al.* 1984).

#### IV. THE SPECTRUM OF THE RE-EMITTED RADIATION

In this section we will calculate the spectrum of the radiation emitted by the grains. In order to do this, we first calculate the grain temperature. Providing the bulk of the emitted radiation is not re-absorbed, a condition which we show is usually fulfilled, the spectrum can be estimated straightforwardly. We confine ourselves to analytic considerations; a proper integration of the radiative transfer equation has been undertaken by Negroponte (1985).

##### (a) Thermal balance

After the pregalactic radiation has been absorbed, it will be re-emitted with a spectrum which depends on the grain temperature  $T_d$ . Providing the grains absorb and emit their own heat capacity in radiation on a timescale short compared to the cosmological time (but that grains are large enough that radiative equilibrium is not affected by single photons),  $T_d$  will be determined by the balance of emission and absorption. If we assume that only the pregalactic sources and the CBR contribute to the incoming radiation, and if we neglect IR self-absorption and the fact that some of the initial radiation will have already been absorbed, this balance gives

$$\frac{\pi^2}{15} \frac{T_d(t)^4}{1+\beta[\omega_d/T_d(t)]^\alpha} = \int_{t_S}^t \frac{n_S(t')L\alpha(t')^4/\alpha(t)^4 dt'}{1+\beta[\omega_d\alpha(t)/T_S\alpha(t')]^\alpha} + \frac{\pi^2}{15} \frac{T_c(t)^4}{1+\beta[\omega_d/T_c(t)]^\alpha} \quad (4.1)$$

where  $T_c$  is the CBR temperature and

$$\beta = \frac{3!\zeta_4}{(3+\alpha)!\zeta_{4+\alpha}} \quad (4.2)$$

Equation (4.1) is only approximate. The denominators were obtained, as in Eq. (3.8), by evaluating the integrals in the  $\omega \ll \omega_d$  and  $\omega \gg \omega_d$  limits and linearly interpolating. This is a reasonable bridge between the two extreme regimes. Inclusion of prior absorption of some of the source radiation would reduce the integrand by a factor  $\exp\{\bar{\tau}(q,t') - \bar{\tau}(q,t)\}$ . However, (4.1) is a good approximation for the dust which is re-emitting most of the energy.

Our approximation here in assuming uniform  $T_d$  is only valid if, from a dust grain's point of view, an appreciable fraction of the optical radiation impinging on it comes from sources outside its own local concentration of stars. This is equivalent to assuming that at least  $\sim 1/2$  of the UV radiation escapes from a typical source. This is certainly true of galaxies today, and likely to be of pregalactic associations as well. Thus for the higher density, optically thick universe, the spectrum of the reemitted radiation is likely to be relatively insensitive to the dust and source distribution. If this assumption is not valid, then our estimate of the spectrum breaks down and becomes dependent on specific details of the source intensity and evolution, and the dust distribution, especially its density contrast. If dust were in "cocoon" around sources, the radiation would appear at a shorter wavelength today than in this calculation; we are therefore estimating the "softest" spectrum the re-emitted radiation could be expected to have. This limiting case may also be the most plausible.

The presence of the CBR appears in the second term on the right hand side of Eq. (4.1), and ensures that  $T_d$  is *always at least as large as*  $T_c$ . The heating effect of the integral term in Eq. (4.1) will tend to make  $T_d$  larger than  $T_c$ . Indeed the CBR term may be relatively unimportant because one expects the sources (unlike the CBR) to have  $T_S > \omega_d$ . It will be useful to introduce a parameter  $F$  which gives the ratio of the comoving radiation density generated by the sources,  $u_{S*}(t)$ , to the comoving CBR density:

$$F(t) \equiv u_{S*}(t) / \frac{\pi^2}{15} (\alpha T_c)^4 \equiv \Omega_{RS}(t) / \Omega_{CBR}(t), \quad u_{S*}(t) = \int_{t_S}^t n_S(t') L(t') \alpha(t')^4 dt'. \quad (4.3)$$

Eq. (4.1) then implies that the heating effect of the sources at redshift  $z$  will be significant for

$$F(z) \gtrsim 5 \times 10^{-3} \left( \frac{r_d}{0.1 \mu} \right)^\alpha \left( \frac{1+z}{10} \right)^\alpha \left( \frac{10^{3(1-\alpha)}}{4\beta} \right). \quad (4.4)$$

Providing  $T_d$  is well below  $\omega_d$ , Eq. (4.1) has the simple solution<sup>1</sup>

$$\alpha T_d(z) = \alpha T_c(z) \left[ 1 + F(z) \beta \left( \frac{r_d}{0.1 \mu} \right)^{-\alpha} \left( \frac{1+z}{10^4} \right)^{-\alpha} \right]^{\frac{1}{4+\alpha}}. \quad (4.5)$$

← Because of the small value of the exponent,  $T_d$  is never very different from  $T_c$ . When (4.4) is not satisfied, it is almost exactly equal to  $T_c$ ; even when that condition is satisfied,  $T_d$  never exceeds  $T_c$  by more than a factor of 10. (The reason for the small exponent in (4.5) can ultimately be traced to the  $T^4$  law for blackbody radiation.) This shows that the assumption  $T_d < \omega_d$  is well justified, so the calculation is consistent. The fact that  $\alpha T_d$  is nearly constant has important

<sup>1</sup>If the depth is large enough that the optical and UV photons get used up quickly, the effective value of  $F$  in Eq. (4.5) will decrease and so  $T_d$  will fall to  $T_c$ . However, most of the light will be emitted at the temperature corresponding to the initial value of  $T_d$ , the time-integrated spectrum falling as  $\lambda^{-4-\alpha}$ .

implications, since it means that the bulk of the re-radiated refuse of the pre-galactic sources tends to pile up in one waveband. The other notable feature is that this band depends only weakly on various uncertain and ill-determined parameters, such as  $r_d$ .

The significance of these results for present day observations is indicated in the  $(q, \alpha)$  space of Fig. 2. The above analysis pertains to incident radiation to the left of the "photosphere," given by Eq. (3.10). We see that the radiation is unabsorbed only below a critical redshift which, for  $\rho_{id} = 3 \text{ g cm}^{-3}$  and  $r_d = 0.1 \mu$ , is given by  $1+z = 8(\Omega_d - 5h)^{-2/3}$ . A line of  $T_S = 3 \times 10^4 \text{ K}$  has been drawn to show where a typical photon at source will lie in this space. However, if this photon is absorbed, it will generate a large number of IR photons external to the IR photosphere and these will propagate along horizontal trajectories until the present if  $T_d$  is to the right of the (IR) photosphere at that time. These trajectories correspond to the lines  $T_d$  specified by Eq. (4.5); for comparison the line  $q = \alpha T_c$  is also shown. The photons will appear as a far IR background or as distortions in the CBR according to whether or not Eq. (4.4) is satisfied.

### (b) The angle-averaged IR emission

Here we obtain the spectrum of the radiation emitted by the grains, assuming that we are not in the regime where IR self-absorption is important, and that  $\alpha T_d$  is approximately constant. The angle-averaged distribution function at the present time is the solution of the radiative transfer equation (3.2):

$$f(q, t_0) = f_{eq}(q)[1 - e^{-\tau(q, t_S)}] + e^{-\tau(q, t_S)} f(q, t_S); \quad (4.6)$$

for  $\tau \ll 1$  the first contribution just reduces to

$$f(q, t_0) \simeq f_{eq}(q / \alpha T_d) \bar{\tau}(q, t_S) \quad (4.7)$$

The associated integrated energy density is thus smaller than the equilibrium black-body density at temperature  $T_d$  by a factor  $\bar{\tau}(4T_d, t_S)$ :

$$\Omega_{RT} = \beta^{-1} \bar{\tau}(T_d, t_S) (T_d / T_c)^4 \Omega_{CBR} . \quad (4.8a)$$

The input source comoving energy density equals the output grain comoving energy density:  $\Omega_{RT} = \Omega_{RS}(t_S) / (1+z_S)$ .

The observed energy density spectrum associated with Eq. (4.7) has more power at short wavelengths than an equivalent blackbody shape:

$$\Omega_R(\lambda) = 0.04(4\beta)\Omega_{RT} \left[ \frac{x^{4+\alpha}}{e^x - 1} \right], \quad x \equiv q / T_d . \quad (4.8b)$$

It peaks at the comoving frequency  $q \approx (4+\alpha)\alpha T_d$  and hence the wavelength

$$\lambda_{pk} \approx 365 \left[ F^{-1} \left[ \frac{\tau_d}{0.1\mu} \right]^\alpha \left[ \frac{1+z}{10} \right]^\alpha \right]^{\frac{1}{4+\alpha}} \left[ \frac{4+\alpha}{5} (4\beta)^{-\frac{1}{4+\alpha}} 10^{-1.9 \left( \frac{\alpha-1}{4+\alpha} \right)} \right] \mu . \quad (4.9)$$

which depends only weakly on the redshift of emission. If  $\tau_d \gtrsim 10^{-2}\mu$ ,  $\lambda_{pk}$  necessarily exceeds  $200\mu$  for  $\alpha = 1$ ,  $F \lesssim 1$ ; for comparison,  $\Omega_{CBR}$  peaks at  $1400\mu$ . (The *average* energy corresponds to  $2000\mu$  for the CBR, and  $460\mu$  for the grain emission.) The appropriate value to use for  $z$  in Eq.(4.9) is discussed in §5.

Of course, Eq. (4.8) describes only one of three components of the background radiation. There is also the unabsorbed optical background and the unabsorbed CBR (which certainly dominates at long wavelengths). The overall spectrum therefore has three peaks, with Eq. (4.8) corresponding to the middle one. In the limit of high redshift or small IR flux, two of the peaks are almost superposed, so that one expects distortions in the CBR spectrum instead of a distinct far-IR background. These qualitative features appear in numerical calculations of McDowell (1985) and Negroponte (1985).

**(c) Reabsorption of grain radiation**

So far we have assumed that the radiation from the grains is never reabsorbed. This is justified providing the opacity given by Eq. (3.9) is less than 1 when  $\lambda_*$  is replaced by the wavelength associated with the grain radiation. Eqs. (4.9) and (3.10) imply that re-absorption will be negligible for

$$1 + z < 65(\Omega_d \cdot 5h\Omega^{-1/2}(\rho_{1d}/2))^{-10/23} \left( \frac{\tau_d}{0.1\mu} \right)^{2/23} F^{-2/23}. \quad (4.10)$$

(For simplicity, we have adopted  $\alpha = 1$ .) This redshift is insensitive to moderate variations in  $\tau_d$  and  $F$ , but is quite sensitive to the grain abundance. Indeed, we can view Eq. (4.10) as defining a relationship between  $\Omega_d$  and  $z$ , the upper boundary of the shaded region in Fig. 3. The shaded region therefore defines the domain of validity of Eq. (4.5). Below this region, the pregalactic light is unaffected, whereas it is at least partially thermalized (reabsorbed) above it.

If reabsorption could occur at centimeter wavelengths, the CBR could itself derive from grains (Layzer and Hively 1973). However, as pointed out by these authors and emphasized by Wright (1982), it requires an implausibly large abundance of "normal" grains for thermalization to be achieved at centimeter wavelengths or longer. (A much smaller abundance is required if the grains are very elongated conducting needles.) As shown in Fig. 3, the most probable situation even in the submillimeter region is that the pregalactic light will be absorbed by the grains but not re-absorbed. This was generally true in models to explain the Woody & Richards (1981) results (Rowan-Robinson, Negroponte, and Silk 1979; Puget and Heyvaerts 1980; Negroponte, Rowan-Robinson, and Silk 1981); these models characteristically produced an optical depth  $\tau \approx 0.1$  near the CBR peak, where the distortion was observed. Other discussions of thermalizing in the microwave region may be found in Wickramasinghe et al (1975), Rees (1978b), and Rana (1981).

## V. ANISOTROPIES: GENERAL CONSIDERATIONS

Anisotropy is introduced by inhomogeneities in the dust density, dust emission properties, and dust temperature. Only the first of these is considered here. This is because one can imagine situations, such as the case where all of the dust is formed well after the bulk of the radiation (so that all of the dust at a particular epoch receives similar irradiation), in which one or both of the other effects are small; but one generally expects that the dust will be inhomogeneous if the matter is. Another good reason for concentrating on this source of anisotropy is that a number of approximations are often valid which considerably simplify the treatment of radiative transfer.

### (a) Extent of the IR emission shell

Photons arriving at the earth  $(x_0, t_0)$  from the direction  $-\hat{q}$  have a distribution function given by the solution to Eq. (3.2)

$$f(q, \hat{q}, x_0, t_0) = e^{-\tau_{\hat{q}}(\chi_i)} f(q, \hat{q}, \chi_i) + \int_{\chi_i}^1 \frac{d\alpha}{\alpha} V_{\hat{q}}(\chi) \left[ f_{*q}(q, \hat{q}, \chi) + \frac{P_S(q, \hat{q}, \chi)}{\Gamma_{\alpha}(q, \hat{q}, \chi)} \right]. \quad (5.1)$$

These photons propagate along the light-cone trajectories  $x(\alpha) = x_0 - \hat{q}\chi(\alpha)$  from the point of emission to the point of absorption (if any). The comoving distance out to redshift  $z$ ,

$$\chi(\alpha) = \int_t^{t_0} \frac{cdt}{a(t)} = \begin{cases} 2H_0^{-1}(1-\alpha^{1/2}), & \Omega=1 \\ 2H_0^{-1}\Omega^{-1/2} \ln \left[ \frac{1+\sqrt{\alpha_0+1}}{\alpha^{1/2}+\sqrt{\alpha_0+\alpha}} \right], & \alpha_0 \equiv \frac{\Omega}{1-\Omega}, \quad \Omega < 1 \end{cases}. \quad (5.2)$$

can be used as a time coordinate;  $\chi_i$  refers to some point before dust creation.

The visibility function

$$V_{\hat{q}}(\chi) = -\frac{d(1-e^{-\tau_{\hat{q}}(\chi)})}{d \ln \alpha} \quad (5.3)$$

picks out the region of greatest change in the depth to grains, and the combination  $V_{\bar{g}} f_{sg}$  determines where the bulk of the emission occurs.

For the case of the microwave background radiation, the onset of recombination causes the depth to be very small just after recombination, and very large just before it, so the visibility function is sharply peaked. The result is a fairly well-defined last scattering surface, with a thickness only  $\sim 10-100$  Mpc.

The fuzziness of the effective surface of emission is much larger in extent in the grain case. At high redshift,  $V$  vanishes, rising up to some peak value as grain production occurs, then falling off as  $\tau \sim a^{-5/2}$  for  $\alpha = 1$  [Eq. (3.9)] once the grain abundance has ceased to change dramatically. If the peak occurs at  $z_{dp}$ , then a reasonable estimate of the comoving length scale over which grain emission may be copious is

$$\begin{aligned} \Delta\chi &= -\frac{d\chi}{d\ln a} = \chi_H \Omega^{-1/2} a^{1/2} / 2 \\ &= 950 (\Omega h^2)^{-1/2} \left( \frac{1+z_{dp}}{10} \right)^{-1/2} \text{ Mpc} , \end{aligned} \quad (5.4)$$

where

$$\chi_H = 2H_0^{-1} = 6000 h^{-1} \text{ Mpc} \quad (5.5)$$

is the current horizon size for  $\Omega = 1$ . We have assumed that  $a_{dp} \ll a_0$  in Eq. (5.4). The average number of galaxies intercepted across this logarithmic redshift interval is

$$\begin{aligned} \frac{dN_G}{d\ln a} &= (n_{G*} \pi R_G^2 / a^2) d\chi / d\ln a \\ &= 0.3 \left( \frac{n_{G*}}{0.01 h^3 \text{ Mpc}^{-3}} \right) \left( \frac{R_G}{10 \text{ kpc}} \right)^2 (\Omega h^2)^{-1/2} \left( \frac{1+z_{dp}}{10} \right)^{3/2} \end{aligned} \quad (5.6)$$

where the subscript  $*$  refers to comoving quantities. As discussed in Sec. 3, it is not implausible that this number can be in excess of one. If it is significantly larger than one, the emission surface can in principle be substantially narrower than the estimate Eq. (5.4), since the emission is governed by the combination  $V_{\bar{q}} f_{*q}$  rather than by  $V_{\bar{q}}$  alone.  $f_{*q}$  is a function of  $aT_d$  which depends only weakly on redshift [ $\sim(1+z)^{-1/5}$  if  $\alpha = 1$ ] unless the depth to the UV and optical is large, in which case  $aT_d$  drops as  $\exp[-(\tau_{UV}(z_i) - \tau_{UV}(z))/5]$  until it reaches the CBR temperature. (The subscript UV denotes the high frequency limit for the depth.) For a given frequency observed today,  $q$ ,  $f_{*q} \sim \exp[-q/aT_d(t)]$  could therefore become quite small. In general, the peak emission shell will depend upon frequency; for example, low frequencies will predominantly arise from those regions where  $aT_d$  is small due to the drop in the comoving source energy density. Such a region occupies a shell characterized by a function of frequency,  $z_{dp}(q)$ , determined by the point at which the IR luminosity at given  $q$  peaks [ $d^2f/d\chi^2 = d(\Gamma_d a e^{-\tau_{\bar{q}}} f_{*q})/d\chi = 0$ ]. This condition is relatively complicated in the general case. Instead, we determine the redshift at which most of the IR energy is emitted.

Due to the overall emission-absorption balance, the bulk of the emission occurs from the region where most of the UV and optical radiation is absorbed. Indeed, the comoving IR density is related to the energy density of the sources by the conservation law for total comoving energy density,

$$u_{IR*}(t) + u_{S*}(t) = u_{S*}(t_i), \quad (5.7)$$

provided most of the source production occurs before grain re-emission. More generally, the right-hand side is replaced by  $\int (\dot{u}_{S*}(t))_{(prod)} dt$ , the time integral of the production rate of source energy density. If Eq. (5.7) is valid, then

$$u_{IR*}(t) = (1 - e^{-\Delta\tau_{UV}(t)}) u_{S*}(t_i).$$

$$\Delta\tau_{UV}(t) = \tau_{UV}(t_i) - \tau_{UV}(t). \quad (5.8)$$

The redshift of maximum emission is therefore  $z_{dp}$  where the comoving IR energy density generated over the comoving length  $d\chi$ ,  $(du_{IR*}(t)/d\chi)d\chi$ , peaks. Since

$$d^2u_{IR*}/d\chi^2 = + \frac{du_{IR*}}{d\chi} \left[ - \frac{d \ln \alpha}{d\chi} \right] \left[ \frac{\Gamma_{aUV}(\alpha)}{H(\alpha)\Omega^{1/2}} + 2 - d_1 \right], \quad (5.9)$$

$$d_1 \equiv \frac{d \ln n_{d*}(\alpha)}{d \ln \alpha}, \quad (5.10)$$

the redshift is determined by setting the quantity in square brackets to zero. The solution is very dependent upon the comoving grain production rate  $d_1$ . In particular, if  $d_1 < 2$ , then  $u_S(t)$  would control the shape of the shell. If the grains were to suddenly appear at redshift  $z_d$ , then  $z_{dp} = z_d$ .

The fuzziness of the emission occupies a comoving width  $\Delta\chi \simeq 2\sigma_\chi$  about the peak distance  $\chi_{dp}$ , where

$$\sigma_\chi = \left| \frac{d^2}{d\chi^2} \ln \left| \frac{du_{IR*}}{d\chi} \right| \right|_{\chi_{dp}}^{-1/2} = \left| \frac{d\chi}{d \ln \alpha} \right|_{\chi_{dp}} |d_1^2 + 3 - 7/2d_1 - d_2|^{-1/2},$$

$$d_2 \equiv \left[ \frac{d^2 \ln n_{d*}}{d \ln \alpha} \right]_{\alpha_{dp}}. \quad (5.11)$$

If we ignore abundance changes at  $z_{dp}$ , ( $d_1 = d_2 = 0$ ),  $\Delta\chi = (2/\sqrt{3}) |d\chi/d \ln \alpha|_{dp}$ , essentially the value of Eq. (5.4). If  $d_1 \gg 2$  at peak, then the fuzziness of the emission surface becomes  $\sim \sqrt{3}/d_1$  narrower. For plausible choices, (5.4) again provides a good estimate. (The width of the emission might also depend on the evolution of source luminosity, but would typically still be of order 1 in  $\log z$ .)

The angular fluctuations in the dust distribution in this emission shell determine the level of anisotropy in the infrared background. These fluctuations are generally higher the narrower the shell. The shell thickness estimated by Eq. (5.4) is generally expected to be significantly larger than the correlation length for the dust (Gpc compared with Mpc). Angular correlations thus reflect dust autocorrelations but are diluted by statistical cancellation along a line of sight. In Sec. 6, we find the anisotropies would be typically at the percent level for arcminute beams. It is worth noting that, if the dust or molecular emissivity has sharp spectral features, the effective width of the emission shell may be reduced by using a narrow-band detector (Hogan & Rees 1979). The fractional anisotropy may be increased in this way by a factor up to  $(\delta\lambda/\lambda)^{-1/2}$ .

**(b) Assumptions in modeling anisotropies**

To simplify the mathematics, we will make the following approximations in discussing the statistics of the random variable  $f$  given by Eq. (5.1): (1) We neglect the initial input  $f(q, \hat{q}, x_i)$ . (2) We ignore the non-grain emission  $P_S$ .  $\rightarrow$  (3) We assume that  $f_{*q}$  is approximately time-independent over the epoch of dominant grain emission. This last point results in a major simplification, and is justified by Eq. (4.5) which shows that  $\alpha T_d$  varies as the one-fifth power of the expansion factor, provided the comoving energy density created by the optical and UV sources does not change by a large factor in less than an expansion time.

With the above three assumptions, the distribution function for the IR emission reaching us takes the simple form:

$$f(q, \hat{q}, x=0) = (1 - e^{-\tau_{\hat{q}}(x_i)}) f_{*q}(q) . \quad (5.13)$$

Thus, the statistics of  $f$  are entirely embodied in those of  $\tau_{\hat{q}}$ . [The general case would include  $\alpha T_d(x, t)$  variations.] Notice that if  $\tau_{\hat{q}} \gg 1$  along a line of sight, a

black-body distribution would be seen coming from that direction.

We now suppose that over the angular resolutions we are interested in the depth in the IR is small, so  $f = \tau_{\vec{q}} f_{\bullet\vec{q}}$ .  $\tau_{\vec{q}}$  is related to a time integral of the grain density, which we can model by the "shot-noise" distribution:

$$n_d(\vec{x}, t) = \int n_{dG}(\vec{x} - \vec{x}', t) n_G(\vec{x}', t) d^3x' . \quad (5.14)$$

Here,  $n_{dG}$  gives the distribution of dust in a given galaxy, and  $n_G$  is the random density field of the galaxies:

$$n_G(\vec{x}, t) = \sum_G \delta^{(3)}(\vec{x} - \vec{x}_G(t)) . \quad (5.15)$$

Provided the angular scale corresponds to a length scale exceeding that of the galactic grain distribution, so that the spatial Fourier transforms of the number densities obey

$$n_d(k) = \frac{\bar{n}_d}{\bar{n}_G} n_G(k) , \quad kR_G / a \ll 1 ,$$

where  $R_G$  is the radius of the dust in the galaxy, the grain density and galaxy density statistics will be identical. The point process for the distribution of the position of the galaxy centers,  $\vec{x}_G(t)$ , is best characterized by a hierarchy of  $N$ -point correlation functions (Peebles 1980).

The angle-average of Eq. (5.13) is, of course, Eq. (4.7). The combination of the  $\chi$ -integral with the angular integral can be used to set up shells which have sufficient volume that the galaxy density averaged over the shell will exhibit only small statistical fluctuations. If we denote the fractional number density fluctuation by  $\delta_G = (n_G - \bar{n}_G) / \bar{n}_G$ , then the fluctuation in the IR distribution function from the angle-average is

$$\Delta f(q, \vec{q}, \chi=0) = \int_0^{x_1} K(t) \bar{n}_G(t) \delta_G(\vec{x} = -\vec{q}\chi, t) d\chi . \quad (5.16a)$$

where

$$K(t) = \frac{\bar{n}_d(t)}{\bar{n}_G} \frac{\sigma_d c q}{\omega_d} f_{dq}(q, t). \quad (5.16b)$$

If we recall that the specific intensity,  $i_\nu \equiv d^2 I_\nu / d\nu d\Omega$ , is related to  $f$  by  $i_\nu = q^4 f / (4\pi^3)$ , and use Eq. (3.4) for the IR luminosity density, then we can cast Eq. (5.16) into the more conventional form

$$\Delta(i_\nu) = \frac{1}{4\pi} \int_{t_0}^{t_0} (1+z)^{-4} \Delta \mathcal{L}_d dt. \quad (5.17)$$

## VI. THE IR CORRELATION FUNCTION

For the (limited) angular resolutions of primary interest to us, the statistics are embodied in the 2-point intensity correlation function. This is the angular correlation of the column comoving luminosity density, Eq. (5.17), which Shectman (1973, 1974) and Peebles (1980) have discussed for optical light. We calculate the 2-point function for various model problems in this section.

### (a) Scaling of fluctuations with resolution angle

Before embarking on a rigorous discussion of the angular structure of the anisotropy it is useful to outline the general behavior one expects. As a model of the dust distribution, suppose that the universe is divided into cells of comoving size  $x_0$  and that the total emission from each cell (i.e., the total amount of dust) is uncorrelated, with  $\langle (\delta \bar{I} / \bar{I})^2 \rangle_{\text{cells}} \simeq 1$  for the ensemble. Within each cell suppose the dust is at uniform temperature but has a clustered structure with correlation function  $\xi(x) = (x/x_0)^{-\gamma}$ . Let  $\theta_0$  be the angle subtended by  $x_0$ . For  $\sigma > \theta_0$ , we have white noise intensity fluctuations in a beam of size  $\sigma$  (§6(e) below)

$$\langle (\delta I / I)^2 \rangle^{1/2} \simeq N^{-1/2} \simeq (x_0 / ct)^{1/2} (\sigma / \theta_0)^{-1} \quad (\sigma > \theta_0), \quad (6.1)$$

where  $N_\sigma$  is the number of cells in a beam of size  $\sigma$  within the emission shell. This is the form of anisotropy most likely to be observed with instruments having resolution worse than  $\approx 1$  arc min ( $\theta_0$  for  $x_0 = 2 \text{ Mpc}(1+z)^{-1}$ ).

However, better resolution can probe statistical properties of structure on smaller scales, even if many cells lie along a line of sight. For  $\sigma < \theta_0$ , we use the following scaling argument. At resolution  $\sigma$ , the distribution "breaks up" into clouds of size  $r_\sigma$ . The cross section for hitting one is  $r_\sigma^2$ . The number density of these clouds is  $n_\sigma = (\rho r_\sigma^3)^{-1}$  (the reciprocal of the mass of each cloud), so the mean number intersected by a beam  $N \propto n_\sigma r_\sigma^2 x \rho^{-1} r_\sigma^{-1}$ . The effective density of each cloud  $\rho$  goes like  $\xi(r)$ , so  $N \propto r_\sigma^{\gamma-1}$ . As before, the variance in intensity goes like  $N^{-1}$ , so

$$\langle (\delta I / I)^2 \rangle^{1/2} \simeq N^{-1/2} \simeq (r_\sigma / ct)^{1/2} (\sigma / \theta_0)^{\frac{1-\gamma}{2}} \quad (\sigma < \theta_0). \quad (6.2)$$

### (b) Intensity autocorrelation function

We now derive the same result using more rigorous methods, which permit a more precise normalization. (The final results for single-beam fluctuations are given in §6(f).) The autocorrelation of the random variable (5.16) is given by

$$\langle \Delta f_{\hat{q}_1} \Delta f_{\hat{q}_2} \rangle = \quad (6.3)$$

$$\int_0^{x_1} d\chi_1 \int_0^{x_1} d\chi_2 K(\chi_1) K(\chi_2) \bar{n}_C(\chi_1) \bar{n}_C(\chi_2) \langle \delta_C(-\hat{q}_1 \chi_1, t_1) \delta_C(-\hat{q}_2 \chi_2, t_2) \rangle.$$

To evaluate this, we assume that we can replace the light cone autocorrelation by an equal time correlation. This is certainly justified. The equation for the  $\Delta f$  correlation is very similar to Limber's equation:

$$\langle \Delta f_{\hat{q}_1} \Delta f_{\hat{q}_2} \rangle = \int_0^{\chi_1} d\chi_1 K^2(\chi_1) \bar{n}_G^2(\chi_1) I(\chi_1 \sin \theta, \chi_1),$$

$$I = \chi_1 \sin \theta \left[ \int_0^{(\chi_H/\chi_1) \sec \theta - \cot \theta} + \int_0^{\cot \theta} \right] dy \xi_G(x = \chi_1 \sin \theta \sqrt{y^2 + 1}, t_1), \quad (6.4)$$

where we have transformed the  $\chi_2$ -integral into one over

$$y = \frac{\chi_2}{\chi_1 \sin \theta} - \cot \theta = \left[ \left( \frac{x}{\chi_1 \sin \theta} \right)^2 - 1 \right]^{1/2}.$$

Here, the comoving distance from the point  $\chi_1$  to a point on the  $\chi_2$ -ray is  $x$ . The galaxy-galaxy correlation function,  $\xi_G(x, t) = \langle \delta_G(\vec{x} + \vec{x}', t) \delta_G(\vec{x}', t) \rangle$  is assumed to be a function of  $|x|$ .

We now introduce  $C(\theta)$  for the fractional intensity correlation function, following the notational convention used in cosmic background radiation studies:

$$C(\theta) = \langle \Delta f(q, \hat{q}_1, \chi=0) \Delta f(q, \hat{q}_2, \chi=0) \rangle / \bar{f}(q)^2. \quad (6.5)$$

Here,

$$\bar{f} = \int_0^{\chi_1} d\chi K(\chi) \bar{n}_G(\chi) \quad (6.6)$$

is the angle-averaged emission. [This  $C$  differs by a factor of 16 from that used in the CBR studies of  $\Delta T/T$  correlations. The  $C$  introduced by Peebles (1980, §58) has dimensions of the square of specific intensity.] The Limber's equation for the angular projection of the galaxy correlation function,  $w(\theta)$ , would have extra powers of  $\chi$  plus a selection function in the integrands, but otherwise the equation is identical to that for  $C(\theta)$ .

**(c) Power law model for the galaxy correlation function**

In this subsection, we adopt a power law form for the galaxy correlation function to illustrate the solution to Eq. (6.4):

$$\xi_G(x, t) = (x_0(t)/x)^\gamma. \quad (6.7)$$

Here, the comoving scale of nonlinearity  $x_0(t)$  may be time dependent (see below). Since the upper limits of integration in the expression for  $I$  in Eq. (6.1) are usually large, we can ignore detailed boundary effects and replace both upper ranges by infinity. Therefore, we immediately obtain a power law expression in  $\sin\theta$  for  $I$ :

$$I = 3J\chi_1(x_0/\chi_1)^\gamma \sin^{1-\gamma}\theta,$$

$$J = \frac{1}{3} \int_0^\infty \frac{dy}{(y^2+1)^{\gamma/2}} = \frac{\sqrt{\pi}}{3} \frac{\Gamma\left(\frac{\gamma-1}{2}\right)}{\Gamma(\gamma/2)} \quad (6.8)$$

$$\approx 1.2 \text{ for } \gamma = 1.8.$$

This leads to an intensity correlation function  $C(\theta) \sim \theta^{-(\gamma-1)}$  for small angles. This does not depend upon the specific history of the emission. The  $\theta^{-(\gamma-1)}$  behavior of  $w(\theta)$  for power law correlation functions arises in exactly the same way.

**(d) Normalization for the correlation amplitude**

To obtain the normalization for this power law requires further assumptions in order to allow evaluation of the time integral. We also now assume the following in addition to (1)-(3) of section V(b): (4) The redshifts  $z_{d1}$  and  $z_{d2}$  over which the IR emission is large are both  $\gg \Omega^{-1}$ . (These redshifts encompass  $z_{dp}$  of peak

emission.) (5) The comoving density of infrared emitting galaxies is time independent over this redshift regime. (6)  $K$  [Eq. (5.16b)] may be taken to be time independent over this redshift interval. (7) The galaxy correlation function (6.7) evolves in a self-similar fashion with a power law dependence on redshift:

$$(x_c(t))^\gamma = a^p(t)(x_c(t_0))^\gamma. \quad (6.9)$$

Peebles (1980, §56.20) adopts  $p = 3 - \gamma + \varepsilon$ , where  $\varepsilon$  is a constant to describe the nonlinear evolution of  $\xi_c$ . Stable bound systems, such as galaxies or virialized groups, give  $p = 3 - \gamma$ ,  $\varepsilon = 0$ . For linear evolution of the correlation function,  $p = 2$ .

With these assumptions, the time integral can then be performed exactly in terms of hypergeometric functions, but this is not a very useful form to work with. A reasonable approximation to the integral, which is valid for all realistic cases, is:

$$\bar{f}^2 C(\theta) = \frac{K^2 \bar{n}_{G^*} a_{d1}^{-3} \left( \frac{\chi_H a_{d1}^{1/2}}{\Omega^{1/2}} \right) x_c(0)^\gamma a_{d1}^\gamma}{2 \left( \frac{11}{2} - p \right)} \frac{1}{\chi_2^{\gamma-1} \sin^{\gamma-1} \theta} \left[ 1 - \left( \frac{a_{d1}}{a_{d2}} \right)^{\frac{11}{2} - p} \right] \quad (6.10)$$

We should compare this fluctuation level with the mean background; in this model,

$$\bar{f} = \frac{K \bar{n}_{G^*} a_{d1}^{-3} \chi_H}{5 \Omega^{1/2}} a_{d1}^{1/2} \left[ 1 - \left( \frac{a_{d1}}{a_{d2}} \right)^{5/2} \right]. \quad (6.11)$$

Thus, the fractional rms fluctuations at a given point will be

$$C(\theta) \equiv \left( \frac{\theta_c}{\theta} \right)^{\gamma-1}$$

$$= \frac{25}{2 \left( \frac{11}{2} - p \right)} \frac{\chi_{d1} \sin \theta}{\chi_H \Omega^{-1/2} a_{d1}^{1/2}} \xi_C(\chi_{d1} \sin \theta, t_{d1}) \frac{[1 - (a_{d1}/a_{d2})^{\frac{11}{2}-p}]}{[1 - (a_{d1}/a_{d2})^{5/2}]^2}. \quad (6.12)$$

Since  $\chi_{d1}\theta$  is the distance along the shell, and  $\Delta\chi \sim \chi_H \Omega^{-1/2} a_{d1}^{1/2}$  [Eq. (5.4)] is the emission surface thickness,  $C(\theta)$  is just the galaxy correlation function times the ratio of the arc to the shell thickness. This latter factor (due to many uncorrelated regions along a beam), substantially lowers the correlation amplitude. The angle subtended by the correlation length  $x_0(t_{d1})$  is

$$\theta_0(t_{d1}) = x_0(t_{d1})/\chi_{d1} = 2.9' a_{d1}^{\frac{1}{2}(\gamma-1)} (1 - a_{d1}^{1/2})^{-1} \left( \frac{x_0(0)}{5h^{-1} \text{Mpc}} \right) \Omega^{1/2}, \quad (6.13)$$

leading to the expression

$$C(\theta) \simeq \frac{25}{8 \left( \frac{11}{2} - p \right)} \left( \frac{x_0(t_{d1}) a_{d1}}{c t_{d1}} \right) \left( \frac{\theta_0(t_{d1})}{\theta} \right)^{\gamma-1}. \quad (6.14)$$

For the specific power law model we can estimate the correlation angle  $\theta_c$  at which the rms fluctuation level reaches unity:

$$\theta_c \approx \theta_0 \left( \frac{x_0(t_0)}{c t_0} \right)^{\frac{1}{\gamma-1}} a_{d1}^{\frac{1}{2} \left( \frac{\gamma-1}{\gamma} \right) \left( \frac{11}{2} - p \right)}. \quad (6.15)$$

For the special case of  $\gamma = 1.8$  and  $x_0(t_0) = 5h^{-1} \text{Mpc}$ , the explicit value is

$$\theta_c = \frac{0.12' a_{d1}^{0.7p-0.6}}{(1 - a_{d1}^{1/2})}. \quad (6.16)$$

The overall amplitude is therefore quite sensitive to clustering evolution parameters  $p$  and  $\gamma$ , and, for some  $p$ , to the redshift at which dust appears. (On the other hand, for  $\gamma = 1.8$  and  $\varepsilon = 0$ , the exponent of  $a$  is only 0.2.)

The case of a burst of infrared radiation which accompanies galaxy formation can be illustrated in this model by taking  $\Delta \ln a = \ln(a_{d2}/a_{d1}) = 2\sigma_\chi |d \ln a / d\chi|$ , where  $\sigma_\chi$  is given by Eq. (5.11):

$$C(\theta) \approx \left\{ \frac{\chi_{dp} \theta}{[(\chi_H \Omega^{-1/2} a_{dp}^{1/2})/2] \Delta \ln a} \right\} \left( \frac{x_0(t_{dp})}{\chi_{dp} \theta} \right)^{\gamma} \quad (6.17)$$

These results break down if the predicted  $\theta_c$  is less than the mean projected separation  $\theta_{sep}$  of galaxy centers in the sky, in which case pointlike galaxies would obviously produce  $C(\theta_{sep}) \approx 1$  ;

$$\theta_{sep} \approx \sqrt{3} \left( \frac{x_g}{\chi_{dp}} \right)^{3/2} \approx 0.8'' \left( \frac{x_g}{\text{Mpc}} \right)^{3/2} \Omega^{3/4} [1 - a_{dp}^{1/2}]^{-3/2} \quad (6.18)$$

Here  $x_g = n_g^{-1/3}$  is the comoving separation between galaxies,  $x_g \approx 4.8h^{-1}\text{Mpc}$  being the mean separation of bright galaxies. In this case galaxy discreteness dominates the anisotropy at small angles. There is also an angle at which the finite size of a galaxy becomes important, for then the correlation function power law will saturate at some sort of "core radius," which we assume is the galactic radius. If galaxies have proper size  $R_G$ , then this angle is redshift-dependent, given by

$$\theta_G = R_G / (a\chi(a)) = 3.4'' \left( \frac{1+z}{10} \right) \left( \frac{R_G}{10 \text{ kpc}} \right) (\Omega h^2)^{1/2} (1 - a^{1/2})^{-1} \quad (6.19)$$

Of course, our treatment is still valid even for these cases as long as one regards (6.7) as the *dust* autocorrelation function. For example, an appropriate model for dust clustering might be to adopt  $\gamma = 2$ ,  $p = 3$ ,  $\chi_0(t_0) \approx 10h^{-1}\text{Mpc}$ , which roughly corresponds to stable galaxies with a present-day (dust) density contrast of  $10^6$  on the scale  $10h^{-1}\text{kpc}$ . (6.15) then takes the particularly simple form

$$\theta_c \simeq \theta_0 \left( \frac{x_0}{ct_0} \right) \quad (6.20)$$

with no  $\alpha$ -dependence. This closely approximates the discrete galaxy model at small  $\theta$  because it predicts  $\theta_c \simeq 0.5''$ , although the larger-angle behavior differs because of the different clustering. Two sample models are shown in Figure 5: one which is anisotropic only because of protogalaxy discreteness, one which includes clustering.

**(e) Finite resolution effects**

In a realistic experiment, the resolution will be finite, either due to telescope limitations (diffraction limited observations) or to imaging on pixels having some resolution scale. Typically, the pixels are designed to have resolution at the level of the diffraction limit. This will probably be the case with SIRTf. (The resolution of IRAS was, however, determined by detector-width.) The intensity fluctuation is then convolved with a resolution function  $F(\hat{q}-\hat{q}')$ , where  $\hat{q}$  denotes the beam center and  $\hat{q}'$  denotes the photon directions:

$$(\Delta f)_F(q, \hat{q}, \chi=0) = \int d\Omega_{\hat{q}'} F(\hat{q}-\hat{q}') \Delta f(q, \hat{q}', \chi=0). \quad (6.21)$$

We refer to this convolution as beam smearing whether it is due to telescope or pixel resolution.

The photon trajectories are rays characterized by the direction  $-\hat{q}$ , which define coordinates on a sphere. Thus we can envisage a sphere in the sky upon which the intensity distribution is imprinted. Provided the distance to the sphere is much less than the distance to the emission shell, this distribution directly gives the pattern we receive. Smearing corresponds to the filtering of small angular scale structure on this sphere. Diffraction-limited observations thus smooth this sky brightness pattern over the resolution scale,  $\sigma$ . A lattice of

pixels in the focal plane of the telescope defines a grid on the sphere which quantizes the smoothed brightness into intensities averaged over angular boxes. The lattice-work may be fixed on the sphere, as in imaging observations, or sweeping across the sphere, as in drift scan measurements. In some cases, it may be considered useful to add the intensities of many nearby pixels together, for example to decrease noise. This corresponds to smearing over a larger scale, so we may treat the resolution scale as a variable.

The evaluation of the smoothed intensity autocorrelation between two directions separated by an angle  $\theta$  requires smoothing of the intensity structure in each of the two directions, involving two integrations over the sphere. The product of the intensity fluctuations in the two patches is then averaged over all of the 2-sphere, with the separation angle  $\theta$  being held fixed to obtain the average autocorrelation. We have implicitly done the second spherical averaging by utilizing the galaxy correlation function, which is volume averaged over a spherical spatial shell at a given redshift. (The shell thickness must be large enough to contain many galaxies;  $\Delta z \sim 1$  suffices.)

The precise form of the beam smearing function is specific to the instrument used, and can be quite complicated. To illustrate the effects of beam smearing, we adopt a Gaussian form with angular dispersion  $\sigma$  for the smearing function  $F$ :

$$F(\hat{q} - \hat{q}') = \frac{1}{2\pi\sigma^2} \exp\left\{-\frac{|\hat{q} - \hat{q}'|^2}{2\sigma^2}\right\}. \quad (6.22)$$

It is normalized to one when integrated over  $4\pi$  steradians (provided  $\sigma \ll 1$  rad.)

The smeared autocorrelation is then given by (e.g., Wilson and Silk 1980)

$$C(\theta; \sigma) = \int_0^\pi \exp\left[-\frac{(\theta^2 + \theta_1^2)}{4\sigma^2}\right] I_0\left(\frac{\theta\theta_1}{2\sigma^2}\right) C(\theta_1) \frac{\theta_1 d\theta_1}{2\sigma^2} \quad (6.23)$$

where  $\theta$ , the angle between the two beam centers, is assumed small (less than a few degrees). The modified Bessel function of zero argument,  $I_0$ , complicates the evaluation of this integral. Generally it would have to be done numerically. The smoothing angle  $\sigma$  is wavelength-dependent. For IRAS, SIRTf, and projections of LDR's capabilities, we have

$$\begin{aligned} \sigma &\simeq 180'' (\lambda / 100\mu\text{m})^{0.63}, & 10\mu < \lambda < 100\mu\text{m} & \text{IRAS} & (6.24a) \\ \sigma &\simeq 30'' (\lambda / 100\mu\text{m}), & 2\mu < \lambda < 750\mu\text{m} & \text{SIRTf} & (6.24b) \\ \sigma &\simeq 4'' (\lambda / 100\mu\text{m}), & \lambda \gtrsim 50\mu, \sigma \simeq 2'', \lambda < 50\mu\text{m} & \text{LDR} & (6.24c) \end{aligned}$$

DIRBE and FIRAS, which will fly aboard COBE, are optimized to determine the IR spectrum from 1 to  $1.3 \times 10^4 \mu\text{m}$  rather than to determine angular structure: their resolution scales are only  $1^\circ$  and  $7^\circ$ .

At small angular separation, it is possible that the intensities reaching nearby pixels will be correlated, and a complete map of the intensity variations would take this into account. If the beam centers define a grid  $\theta_L$ , where  $L$  runs over a set of integers, then the relevant fluctuations to consider will be those between two pixels:

$$(\Delta f)_{LL'} = (\Delta f)_L - (\Delta f)_{L'} \quad (6.25)$$

The rms fluctuations will depend upon the separation of the grid points:

$$\frac{\langle (\Delta f_{LL'})^2 \rangle}{\bar{f}^2} = 2(C(0;\sigma) - C(\theta_L - \theta_{L'};\sigma)) \quad (6.26)$$

If the separation is smaller than the correlation angle then of course the pixel intensities will be correlated, resulting in a small rms pixel-to-pixel fluctuation. The pixel to pixel variation becomes largest for  $\theta > \theta_0$ , for then the intensities in the two will be uncorrelated, with each contributing the single-pixel rms fluctuation  $C(0;\sigma)^{1/2}$ . This accounts for the factor of two in Eq. (6.26).

(f) Single beam rms fluctuations

Here, we consider the dispersion expected within one beam; that is, we calculate  $C(0; \sigma) = \langle (\delta I / I)^2 \rangle(\sigma)$ :

$$C(0; \sigma) = \int_0^{\infty} e^{-y} dy C(2\sigma\sqrt{y}). \quad (6.27)$$

The power law form of  $C(\theta)$  yields

$$C(0; \sigma) = \left( \frac{\theta_c}{2\sigma} \right)^{\gamma-1} \Gamma\left( \frac{3-\gamma}{2} \right), \quad \Gamma(0.6) = 1.49. \quad (6.28)$$

This demonstrates that the power law remains a  $(\delta I / I)_{\text{rms}} \sim \sigma^{-(\gamma-1)/2}$  law as a function of beam angle. Further, if we use Eq. (6.12) for  $C(\theta)$ , we can write this result in the form:

$$C(0; \sigma) \approx \frac{25}{6(11/2-p)} \Gamma\left( \frac{3-\gamma}{2} \right) \left( \frac{x_0(t_{dp}) \alpha_{dp}}{c t_{dp}} \right) \left( \frac{\theta_0(t_{dp})}{\theta} \right)^{\gamma-1}. \quad (6.29)$$

This is the result obtained in Eq. (6.2) using simple scaling arguments, apart from a numerical factor 1.77 for the  $p = 2$  case. Inserting the parameters of Eq. (6.13) with  $p = 2$ , we obtain intensity fluctuations

$$\begin{aligned} (\delta I / I)_{\text{rms}} &= \sqrt{C(0; \sigma)} = 0.029(1' / \sigma)^{0.4}, \quad z_{dp} = 4 \\ &= 0.016(1' / \sigma)^{0.4}, \quad z_{dp} = 9. \end{aligned} \quad (6.30)$$

However, if  $\theta_0 \lesssim 1'$  [Eq. (6.11)], the form of the dependence would change at (more accessible) larger angles. If  $C$  is approximated by a top hat, going to zero beyond some coherence angle  $\theta_{coh}$ , then

$$\begin{aligned} C(0; \sigma) &= C(0)(1 - \exp[-(\theta_{coh} / 2\sigma)^2]) \\ &\approx C(0)(\theta_{coh} / 2\sigma)^2, \quad \sigma \gg \theta_{coh}. \end{aligned} \quad (6.31)$$

This is the "white noise" result discussed above [Eq. (6.1)], namely that the rms intensity fluctuations scale as  $\sigma^{-1}$  for beams larger than the characteristic coherence length. It is difficult to realize a correlation which will be precisely of this top hat form however.

A truncated power law for  $C(\theta)$  is a more realistic approximation which illustrates the result of a lack of correlation on large angular scales:

$$C(\theta) = (\theta_c / \theta)^{\gamma-1} H(\theta_{coh} - \theta), \quad (6.32)$$

where  $H$  is the Heaviside function. The associated single-beam dispersion involves incomplete gamma functions:

$$C(0;\sigma) = \left(\frac{\theta_c}{2\sigma}\right)^{\gamma-1} \left\{ \Gamma\left[\frac{3-\gamma}{2}\right] - \Gamma\left[\frac{3-\gamma}{2}, \left(\frac{\theta_{coh}}{2\sigma}\right)^2\right] \right\}. \quad (6.33)$$

This expression gives power laws for the intensity fluctuations in the appropriate limits:

$$C(0;\sigma) = \Gamma\left[\frac{3-\gamma}{2}\right] \left(\frac{\theta_c}{\theta_{coh}}\right)^{\gamma-1} \left(\frac{\theta_{coh}}{2\sigma}\right)^{\gamma-1}, \quad \sigma < 0.3\theta_{coh} \quad (6.34a)$$

$$C(0;\sigma) = \frac{2}{3-\gamma} \left(\frac{\theta_c}{\theta_{coh}}\right)^{\gamma-1} \left(\frac{\theta_{coh}}{2\sigma}\right)^2, \quad \sigma > \theta_{coh}. \quad (6.34b)$$

In the ranges indicated, these approximations are excellent fits to the behavior given by Eq. (6.33), as illustrated in Fig. 4.

The important issue for observability is the normalization amplitude  $(\theta_c / \theta_{coh})^{\gamma-1}$ . For the case of galaxies confined to superclusters or pancakes at early times, we might take  $p = 0$ ,  $\Omega = 1$ ,  $\theta_c \simeq 0.6''$ ,  $\theta_{coh} \simeq 5'$ ; hence  $(\theta_c / \theta_{coh})^{(\gamma-1)/2} \simeq 0.08$  in the linear regime of evolution. Thus, we might expect to have considerable correlation power at angular scales  $\sigma \sim \theta_{coh}$ . A

contribute only a modest background flux at  $100\mu\text{m}$ , may produce significant brightness fluctuations. Here we estimate the "confusion limit" of anisotropy measurements: what is the level of fluctuations likely to be produced by unresolved foreground galaxies?

Generally, "confusion" refers to the problem of identifying discrete sources with finite resolution when they become too dense on the sky. Here, we ask whether marginally unresolved discrete sources will contribute more anisotropy than fluctuating background noise which is almost certainly unresolved. The contamination is thus the result of the brightest galaxies which a given telescope just fails to resolve. The following discussion owes much to notes by M. Werner (unpublished).

Let us suppose we know the number  $N_0$  of galaxies on the sky (per sr) brighter than a certain limiting flux  $S_0$ . The usual Euclidean flux-density relation

$$S = S_0(N/N_0)^{-2/3} \quad (7.1)$$

then tells us the brightness cutoff of local sources with some specified surface density  $N$ . [Note that sources at  $z \gg 1$  in a shell of comoving thickness  $\Delta \log z \simeq 1$  are at nearly (to within a factor of order unity) the same luminosity distance. Therefore  $z \gg 1$  sources produce a "spike" in the  $\log N - \log S$  relation: below some limiting flux  $S(z)$ , there is a sudden increase in  $N$ . Significant evolution in the interval  $z \sim 1-3$  just produces a non-Euclidean power-law, as we are already familiar with from the radio source counts. This could also be the case in the infrared, but for simplicity we here divide the sources into "foreground" ones with  $z \ll 1$  and "background" ones with  $z \gg 1$ .]

To estimate the confusion limit of a telescope with aperture  $D$ , we note that its half-power diffraction beamwidth is

$$\theta_D \simeq \lambda / D \simeq 20'' (\lambda / 100\mu\text{m})(D / 1\text{m})^{-1}. \quad (7.2)$$

Sources more numerous than about 1 per  $10\theta_D^2$  will be unresolved and appear as "background fluctuations"; thus, the confusion limit is  $S_{\text{conf}} \simeq S_0(N_{\text{conf}}/N_0)^{-2/3}$  where  $N_{\text{conf}} \simeq 1/10\theta_D^2$ . At present, only rough estimates are available for  $S_0$  and  $N_0$  at long wavelengths (based either on extrapolations from shorter wavelengths, from small samples, or preliminary IRAS results). We use the IRAS numbers (cf. Soifer *et al.* 1984; Houck *et al.* 1985),

$$N_0 \simeq 0.25 \text{ deg}^{-2}, \quad S_0 \simeq 0.5 \text{ Jy}, \quad \lambda = 60\mu; \quad (7.3)$$

and simply adopt the same numbers  $N_0, S_0$  for  $100\mu$ , effectively assuming that the typical spectrum in this region is flat. We then obtain

$$S_{\text{conf}} \simeq 1 \text{ mJy } \lambda_{100}^{4/3} D_m^{-4/3} [S_0(\lambda) / S_0(100\mu\text{m})]. \quad (7.4)$$

Fluctuations  $\delta I$  of this order occur due to foreground galaxies in square "pixels"  $\theta_{\text{conf}} \simeq 3\theta_D$  on a side. Figure 5 shows the bolometric flux corresponding to the confusion limited fluctuation for a 1 m (SIRTF class) telescope at  $100\mu$  and (assuming  $\alpha = 1$  emissivity) at  $300\mu$ . The white-noise fluctuations at  $\theta > 3\theta_D$  are those remaining after identifiable sources are subtracted out; the true total fluctuation on scale  $\theta$  would always be dominated by those with  $N \simeq \theta^{-2}$ .

For this reason, a larger mirror (e.g., LDR) is very useful in removing foreground contaminants, as well as probing interesting angular scales  $\theta_D \lesssim \theta_0$  where clustering properties become important. (Clustering of foreground galaxies has been ignored in the above calculation, and would worsen the situation at small  $\theta$ .)

Now consider, for illustration, a background of  $0.3M \text{ Jy sr}^{-1}$ , i.e.,  $\Omega_R h^2 = 2 \times 10^{-7}$ . If it peaks at  $\sim 100\mu$ , it may be marginally observable as diffuse emission above galactic and zodiacal emission, but its small-scale anisotropy is

invisible to IRAS, and will only be discernable even by SIRTf if the emitting material is quite highly clustered (cf. Fig. 5). If it peaks at  $\lambda 300\mu$ , it should stand out conspicuously above local diffuse sources in COBE measurements, and its anisotropy should dominate foreground galaxies even if the scale of clustering of the emitting material is roughly a galactic scale, with the anisotropy being due entirely to galaxy discreteness. It is also clear that for strongly clustered emitters, the anisotropy of the IRB might be observable above the confusion limit even if the diffuse component itself is unobservable, buried behind local diffuse emission. In this case, deep, high angular resolution surveys would provide the best search technique for detecting the background.

## VII. DISCUSSION AND CONCLUSIONS

Most current cosmological scenarios predict the existence of background radiation in the far infrared. If no such background is detected by COBE, it will imply that the universe was indeed dark during the "dark ages" between  $z \sim 4$  and  $z \sim 1000$ , compared with its luminosity today. This is conceivable, but seems highly unlikely in view of several phenomena which may be indicative of an energetic early universe. High redshift radiation by familiar types of sources would produce a near-infrared background, were it not for the likely presence of obscuring dust. Dust opacity leads to generic averaged spectra which are so insensitive to prevailing conditions that the background spectrum, even if detected, would not necessarily contain useful information about its origin. However, the anisotropy of the radiation would still convey information about the dust distribution and hence about the distribution of matter at high redshift. SIRTf offers a realistic hope of observing this anisotropy. In this section, we summarize our main results and discuss how they may fit into the framework of

current cosmological theories.

(1) *Observational limits and prospects.* It is useful to keep in mind the following benchmarks, expressed in terms of  $\Omega_R h^2$  ; total  
 CBR flux  $\sim 2 \times 10^{-5}$ ; limits on diffuse near-infrared emission  $\sim 4 \times 10^{-4}$ ; limits on  
 diffuse optical and UV backgrounds  $\sim 4 \times 10^{-6}$ ;  $100 \mu$  emission at the galactic  
 poles  $\sim 1 \times 10^{-5}$ , of which about half is zodiacal emission and about half is galactic  
 (Low et al. 1985) or extragalactic (Rowan-Robinson 1985); intrinsic IRAS sensi-  
 tivity  $\sim 10^{-6}$ ; COBE sensitivity  $\sim 3 \times 10^{-8}$  for  $500 \mu < \lambda < 1 \text{ cm}$ ; SIRTF  $\left( \begin{smallmatrix} (100 \mu) \\ \text{sensitivity} \end{smallmatrix} \right) \sim 10^{-8}$ .

(2) *Sources of IR radiation.* In the absence of dust, a near IRB is expected from primeval stars, whether they are pregalactic or form in primeval galaxies. If large scale structure is generated by supernova explosions, the IRB from the main-sequence precursors is expected (cf. eq. 2.22) to have  $\Omega_R \sim 10^{-4}$ . If we exclude this possibility, a reasonable *upper bound* to  $\Omega_R$  (cf. eq. 2.11) corresponds to VMOs producing black holes at a dark matter density of  $\Omega_* \sim 0.1$ :  $\Omega_R \sim 10^{-5}$  for  $z_* \sim 50$ . A *lower bound* arises if we include only those stars required to produce metals (cf. eq. 2.3): to generate Population II abundances at  $z \sim 10$  implies  $\Omega_R \sim 10^{-7}$ ; to generate Population I abundances at  $z < 1$  implies  $\Omega_R \sim 10^{-6}$ . Black hole accretion could also generate  $\Omega_R \sim 10^{-6}$ . A near or far IRB may arise from decaying relics of the Big Bang.  $\Omega_R$  and  $\lambda_{pk}$  are sensitive to the mass, lifetime, and abundances of the particles (cf. eq. 2.25). For example, a 1 keV neutrino decaying at redshift  $\sim 10^5$  would give  $\Omega_R \sim 5 \times 10^{-5}$ .

(3) *Distribution of dust.* The cosmic IR background is probably strongly affected by dust. Dust at early times would most likely be associated with primeval galaxies, but could have a uniform pregalactic component. The best

constraint on the abundance of uniform dust arises from the lack of QSO reddening:  $\Omega_d h < 6 \times 10^{-5}$  (Wright 1982). The clumped dust abundance is much less constrained;  $\Omega_d \sim 10^{-5}$  is typical of that expected in galaxies. Since the optical depth to absorption by dust through a large spiral galaxy is of order one, if such galaxies cover the sky, the universe would be optically thick to dust (Ostriker and Heisler 1984). The redshift when the sky is just covered by galaxies and the redshift when the angle-averaged optical depth reaches unity are both about 10 (eq. 3.9, 3.14).

(4) *Regimes of cosmic radiative transfer with dust.* In many situations, the universe is *thick in the UV and optical* at  $z \gtrsim 5$ , but is *thin in the far-infrared*. As Figures 2 and 3 emphasize, the most likely regimes in  $\Omega_d - z$  space correspond either to total transparency to primeval radiation or to absorption by intervening primeval dust with the degraded re-emitted radiation undergoing transparent transmission.

(5) *The infrared photosphere.* The bulk of the dust absorption and emission would come from a shell localized in redshift,  $\Delta z \lesssim z$ . The position of the far side of the shell is determined by the turn-on epoch for radiation or dust production (whichever comes later), and the position of the near side by the condition that the shell have unit optical depth. The concept of a shell applies if the emission region has comoving thickness significantly less than its comoving distance. For example, if galaxies form at  $z=10$ , the thickness and distance are  $1h^{-1}$  Gpc and  $4h^{-1}$  Gpc, respectively.

(6) *Spectrum of reprocessed radiation.* The output radiation density from the dust is just the input from the sources,  $\Omega_{RS}$ . The peak wavelength of dust radiation, redshifted to the present, is insensitive to parameters (cf. eq. 4.9 with  $\alpha=1$ ):

$$\lambda_{pk} \simeq 688 \mu \left[ \left( \frac{\Omega_{RS} h^2}{10^{-6}} \right) \left( \frac{0.1 \mu}{r_d} \right) \left( \frac{10}{1+z_{dp}} \right) \right]^{-1/5}$$

where the appropriate value to use for  $z_{dp}$  is discussed in Sec.V(a).

Since the CBR peaks at  $1400\mu$ , the peak flux levels for many of the sources discussed above represent a significant excess over the CBR, which has  $\Omega_R(400\mu)h^2 = 6 \times 10^{-7}$  and  $\Omega_R(200\mu)h^2 = 2 \times 10^{-8}$ . Our conclusions regarding the IR spectrum and anisotropy are insensitive to the dust distribution within galaxies, except that if the bulk of the energy sources are shrouded in very dense dust clouds with  $\bar{\tau} > 1$  and a small net covering factor, there may be another component for which  $\lambda_{pk}$  will be less than calculated here.

(7) *Epoch of dust formation.* In the "isocurvature" models of galaxy formation in baryon-dominated universes, much of the universe is expected to form bound objects by  $z \sim 100$  leading to relatively early dust formation. On the other hand, the adiabatic "pancake" models would not form dust until the time of pancake collapse,  $z \sim 5$ . The impact of the dust on the largely optical and UV background radiation would likely be small ( $\bar{\tau} < 1$ ). In cold dark matter models, structures on scales  $\sim 10^7 - 10^{12} M_\odot$  would have formed almost simultaneously, predominantly during the epoch  $z \sim 5 - 20$ . In explosion scenarios, dust obscuration at  $z \sim 5 - 10$  is already observationally *required*.

(8) *Infrared anisotropy at small angular scale.* Statistical fluctuations in the dust distribution and temperature in the shell lead to far IRB anisotropies. If the dust is distributed like galaxies, whose correlation function may be taken to be a power law (cf. eq. 8.7) truncated above the correlation length  $x_0(z)$ , then the fractional rms fluctuations in a single "beam" smeared over a resolution angle  $\sigma$  are  $\Delta I / I \propto \sigma^{-(\gamma-1)/2}$  if  $\sigma < \theta_0$ ,  $\propto \sigma^{-1}$  if  $\sigma > \theta_0$ . Here,  $\theta_0 \simeq 3'$  is the angle subtended at the emission shell by the correlation length. In general there are many regions of scale  $\sim x_0$  across the shell, so the fluctuation amplitudes in the radiation are relatively small. For SIRTf parameters at  $400\mu$ ,  $\sigma \sim 120''$ , the fluctuations are likely to be in the  $\sigma^{-1}$  regime. Typical fluctuation levels would then be  $\Delta I / I \sim 0.02 - 0.07 (1' / \sigma)$ , depending on the evolution of the correlation

function. These fluctuations may, in some circumstances, be seen above the confusion limit associated with the direct IR emission from unresolved foreground (low  $z$ ) galaxies.

#### ACKNOWLEDGEMENTS

We are particularly grateful for informative discussions with R. Hildebrand, J. Negroponte, E. Wright, and members of the IRAS science team, particularly B.T. Soifer, G. Neugebauer, M. Rowan-Robinson, and M. Werner. This work was supported by the NSF under grant PHY77-27084, supplemented by funds from NASA, at the Institute for Theoretical Physics, Santa Barbara, the Theoretical Astrophysics Group at Fermilab, CJH's Bantrell Fellowship and NSF grant AST82-14126 at Caltech, and NASA grant NAGW-299 at Stanford.

#### APPENDIX: COSMOLOGICAL PURCELL'S THEOREM

Suppose that the universe is filled with a space density  $n_d$  of spheroidal grains, each with dielectric constant  $\epsilon_d$ , semiaxis  $a$  along the axis of symmetry, and semiaxis  $b$  along the perpendicular dimension. Let  $P(\lambda)$  be the probability per unit length of a photon of wavelength  $\lambda$  interacting with matter. Purcell (1969) proved that

$$\int_0^{\infty} P(\lambda) d\lambda = 2\pi^2 n_d a b^2 F$$

where  $F(a/b, \epsilon_d)$ , the ratio of the susceptibility of isotropically-oriented spheroids to conducting spheres of the same volume, is of order unity unless the grains are both good conductors and very elongated ( $\log|(a/b)| \gg 1$  and  $\epsilon_d \gg 1$ ; see Wright 1982). Purcell's theorem demonstrates that the probability of absorption or scattering of broad-band radiation is related directly to the total length traversed by a light path through solid matter, and only weakly

depends on the size, composition, and distribution of the matter (indeed, the relation also applies to  $\lambda$ -integrated molecular line emission). Light of wavelength  $\lambda$  must pass through a length  $\simeq \lambda$  of solid material to have a significant chance of absorption or scattering. The integrated optical depth for photons emitted at  $z$  with observed wavelength  $\lambda_0$  is

$$\tau_0(\lambda_0, z) = \int_{t(z)}^{t_0} c dt P[\lambda_0 / (1+z)]$$

Combining these equations with standard cosmology gives a cosmological version of Purcell's theorem,

$$\int_0^{\infty} d\lambda_{\mu} \tau(\lambda_{\mu}, z) = 0.08 F \Omega_0 h \rho_{\text{td}}^{-1} \int_0^z dz' (1+z')^2 (1 + \Omega_0 z')^{-1/2} \Omega_{d,-5}(z')$$

where  $\lambda_{\mu} = \lambda_0 / (1+z)$ . Note that this expression takes account of the possibility of opacity by molecular line emission or any other resonant radiation mechanisms "smeared" into a continuum absorption by cosmological redshift. Some of the conclusions in the text, based on a crude model of dust opacity, thus carry over to smaller grains, large hydrocarbon molecules, or even CO opacity.

## REFERENCES

- Alfvén, H., and Mendis, A. 1977. *Nature*, **266**, 699.
- Begelman, M.C. 1984. Proceedings Santa Cruz Workshop, *Astrophysics of Active Galaxies and Quasi-Stellar Objects*.
- Begelman, M., Blandford, R., & Rees, M.J. 1984. *Rev. Mod. Phys.*, **256**, 255.
- de Bernardis, P., Masi, S., Malagoli, A., and Melchiorri, F., 1985. *Ap. J.*, **288**, 29.
- Bond, H.E. 1981. *Ap. J.*, **248**, 606.
- Bond, J.R., Arnett, W.D., and Carr, B.J. 1984. *Ap. J.*, **280**, 825.
- Bond, J.R., and Szalay, A.S. 1983. *Ap. J.*, **274**, 443.
- Bondi, H. 1952. *M.N.R.A.S.*, **112**, 195.
- Campbell, A., and TerLevich, R. 1984. *M.N.R.A.S.*, **211**, 15.
- Carr, B.J., and Rees, M.J. 1984. *M.N.R.A.S.*, **206**, 315.
- Carr, B.J., Bond, J.R., and Arnett, W.D. 1984. *Ap. J.*, **277**, 445.
- Carr, B.J., McDowell, J., and Sato, H. 1983. *Nature*, **306**, 666.
- Dube, R.R., Wickes, W.C. & Wilkinson, D.T. 1979. *Ap.J.*, **232**, 333.
- Draine, B.T. and Lee, H.M. 1984. *Ap. J.* **285**, 89.
- Erickson, E.F., Knacke, R.F., Tokunaga, A.T., and Haas, M.R. 1981. *Ap. J.*, **245**, 148.
- Ezer, D., and Cameron, A.G.W. 1971. *Ap. Space Sci.*, **14**, 399.
- Faber, S.M., and Gallagher, J.S. 1979. *Ann. Rev. Astr. Ap.*, **17**, 135.
- Fall, S.M., and Tremaine, S. 1977. *Ap. J.*, **216**, 682.
- Fowler, W.A. 1966. *Ap. J.*, **144**, 180.
- Fricke, K.J. 1973. *Ap. J.*, **183**, 941.
- Gush, H.P. 1981. *Phys. Rev. Lett.* **47**, 745.
- Hauser, M.G., *et al.*, 1984. *Ap. J. (Letters)*, **278**, L15.
- Hildebrand, R.H. 1983. *Quart. J.R.A.S.*, **24**, 267.
- Hoffman, W., and Lemke, D. 1979. *Astr. Ap.*, **68**, 389.

- Hogan, C., and Rees, M.J. 1979. *M.N.R.A.S.* **188**, 791.
- Houck, J.R. *et al.* 1985. *Ap. J. Lett.* **290**, L5.
- Iben, I. 1967. *Ann. Rev. Astr. Ap.*, **5**, 571.
- Kashlinsky, A., and Rees, M.J. 1983. *M.N.R.A.S.*, **205**, 955.
- Lacey, C. 1984. in *Formation and Evolution of Galaxies and Large Structures in the Universe*, eds. J. Audouze and J. Tran Thanh Van (Reidel, Dordrecht).
- Layzer, D., and Hively, R. 1973. *Ap. J.*, **179**, 361.
- Low *et al.*, 1985. Paper delivered at AAS meeting, Tucson, January 1985.
- Matsumoto, T., Akiba, M., and Murakami, H. 1984. *COSPAR Journal: Advances in Space Research*, eds. G.F. Bignami and R.A. Sunyaev (Pergamon, Oxford).
- Mathis, J.S., Ruml, W., and Nordsieck, K.H. 1977. *Ap. J.*, **217**, 425.
- McDowell, J. 1985. Preprint, University of Cambridge.
- Negroponete, J. 1985. Unpublished.
- Negroponete, J., Rowan-Robinson, M., and Silk, J. 1981. *Ap. J.* **248**, 38.
- Ostriker, J.P., and Heisler, J., 1984. *Ap. J.*, **278**, 1.
- Palla, F., Salpeter, E.E., and Stahler, S.W. 1984. *Ap. J.*, **271**, 632.
- Peebles, P.J.E., 1980. *The Large Scale Structure of the Universe*, (Princeton University Press).
- Peebles, P.J.E., and Dicke, R.H. 1968. *Ap. J.* **154**, 891.
- Peebles, P.J.E., and Partridge, R.B., 1967. *Ap. J.* **147**, 865; *Ap. J.* **148**, 377.
- Peterson, J.B., Richards, P.L., & Timusk, T. 1985. Berkeley preprint (to appear in *Phys. Rev. Lett.*)
- Pollaine, S. 1978. *Nature* **271**, 426.
- Puget, J.L., and Heyvaerts, J. 1980. *Astr. Ap.*, **83**, L10.
- Purcell, E.M. 1969. *Ap. J.*, **158**, 433.
- Rana, N.C. 1981. *M.N.R.A.S.*, **197**, 1125.
- Rees, M.J. 1978. *Phys. Script.*, **17**, 193.
- Rees, M.J. 1978b. *Nature*, **275**, 35.
- Richards *et al.* 1984. Berkeley Preprint (to appear in *Proc. Inner Space/Outer Space*, ed. M. Turner & E. Kolb, (University of Chicago Press)).

- Rowan-Robinson, M., Negroponte, J., and Silk, J. 1979. *Nature*, **281**, 635.
- Rowan-Robinson, M. 1985. Preprint, Queen Mary College, London.
- Schwartz, P.R. 1982. *Ap. J.* **252**, 589.
- Shectman, S. 1973. *Ap. J.* **179**, 681.
- Shectman, S. 1974. *Ap. J.* **188**, 233.
- Silk, J. 1977. *Ap. J.*, **211**, 638.
- Silk, J., and Stebbins, A., 1983. *Ap. J.*, **269**, 1.
- Soifer, B.T., *et al.* . 1984, *Ap. J. (Letters)*, **278**, L71.
- Stecker, F.W., Puget, J.L., and Fuzio, G.G. 1977. *Ap. J. Lett.* **214**, L51.
- Sunyaev, R.A., Tinsley, B.M. & Meier, D.L. 1978. *Comments Astrophys. Sp. Sci.*, **7**, 183.
- Terlevich, R. 1983. Ph.D. thesis, Cambridge University.
- Thorstensen, J., and Partridge, R.B. 1975. *Ap. J.* **200**, 527.
- Truran, J.W., and Cameron, A.G.W. 1971. *Ap. Space Sci.*, **14**, 179.
- Weaver, T.A., and Woosley, S.E. 1980. *Ann. NY Acad. Sci.*, **336**, 335.
- Weinberg, 1972. *Gravitation and Cosmology* (New York: Wiley).
- Wickramasinghe, N.C., Edmunds, M.G., Chitre, S.M., Narlikar, J.V., and Ramadurai, S. 1975. *Ap. Space Sci.*, **35**, L9.
- Woody, D.P., and Richards, P.L. 1981. *Ap. J.*, **248**, 18.
- Wright, E.L. 1981. *Ap. J.*, **250**, 1.
- Wright, E.L. 1982. *Ap. J.*, **255**, 401.

**FIGURE CAPTIONS**

Figure 1a. — Integrated radiation density as a fraction of the closure energy density, Eq. (1.1), in terms of peak observed wavelength (assuming no dust obscuration) for the following sources: (II9) Massive (metal producing) stars generating Population II abundances ( $Z = 10^{-3}$ ) at  $z = 9$ . (II100) The same, but at  $z = 100$ . (I1) Massive stars at  $z \ll 1$  generating Population I abundances ( $\Delta Z = 10^{-2}$ ). (IMS) The maximum background from non-metal-producing intermediate mass stars. (This scales as  $\Omega_{*x}$ ; we here take  $\Omega_{*} = 0.1$ ). (LMS) The maximum background from low mass stars ( $\lesssim 0.1 M_{\odot}$ ) if these provide the dark matter in halos ( $\Omega_{*} \simeq 0.1$ ). (VMO) Very Massive Objects at  $z = 100$  with  $\Omega_{*} = 0.1$ . (VMBH)  $10^6 M_{\odot}$  black holes with  $\Omega_{*} = 0.1$  accreting from a uniform pregalactic medium at  $z \sim 40$ . (AGN9) Eddington-limited accretion from black holes at  $z = 9$  with  $\Omega_b = 10^{-5}$  appropriate to quasar precursors. (DP) Massive Decaying Big Bang relic particles with  $m_X = 1 \text{ keV}$ ,  $E_X \Omega_X = 10^{-2}$  decaying at redshift  $z_d = 10^3$ . Sample background light limits at 6 wavebands in the optical and near IR are also shown (Carr et al. 1984).

Figure 1b. — Sample spectra for selected cases in 1a. For II9, II100, and I1 a generic  $25 M_{\odot}$  star with 40,000 K was taken. Population III VMOs are at  $10^5 \text{ K}$ . A generic 25,000 K blackbody was taken for N9 as representative of radiation tori thermal emission. Though these spectra indicate typical wavelength spreads, inclusion of a population of objects radiating over a band of redshifts will generally give broader curves. The DP case is, however, exact.

Figure 2.—Absorption and emission by cosmic dust. Observed wavelength  $\lambda$  is plotted against  $(1+z)$ . Thus, unabsorbed photons propagate along vertical trajectories. For constant  $\Omega_d = 10^{-5}$ ,  $\tau_d = 0.1 \mu$ , and emissivity

exponent  $\alpha = 1$ , the shaded line  $\tau = 1$  shows the redshift beyond which an emitted photon (of fixed  $\lambda$ ) would have been absorbed by a grain before reaching the present. We assume  $\Omega = h = 1$ . The peak wavelength of unabsorbed redshifted starlight is shown for  $T_* = 3 \times 10^4$  K. If enough starlight is present to equal the CBR energy density uniformly distributed dust will have an equilibrium temperature  $T_d$  with peak wavelength of emission as shown. For  $10 \lesssim z \lesssim 100$ , the universe is optically thick to emitted starlight, but optically thin to radiation at the peak dust emission frequency; thus, starlight emitted during this period is degraded into an anisotropic nonthermal far-infrared background, described by approximations in the text which ignore dust reabsorption.

Figure 3.—Critical grain abundance as a function of redshift. The shaded region indicates regime where UV photons are absorbed by grains but re-emitted IR is not (the regime of most interest here). The regime above and to the right is thick at the peak emission wavelength of the dust, while the lower region is transparent even in the UV. Limit from observation of high-redshift quasars is shown, assuming uniformly distributed dust. The CBR is thick to the dust at peak above the  $\lambda = 1.4$  mm line; it is thick at the  $\longrightarrow$  Rayleigh-Jeans wavelength  $\lambda = 1$  cm only above the corresponding line.

Figure 4.—The variance of the fractional intensity fluctuations  $\langle (\delta I / I)^2 \rangle(\sigma) = C(0; \sigma)$  in a single beam given by Eq. (6.33) are plotted against resolution angle  $\sigma$ ;  $\theta_{coh}$  is the coherence angle. The low and high  $\sigma$  limit fits are given by Eq. (6.34). A typical coherence angle would be  $4'$  if there is no correlation function evolution, and  $20''$  if there is correlation function evolution with  $p = 2$  [Eq. (6.13)]. For the latter case, the resolution angles of IRAS, SIRTf, and LDR are shown, at  $\lambda = 100 \mu$ , as well as the angles subtended by galaxies of 10 kpc

radii. The normalization amplitude,  $(\theta_c / \theta_{coh})^{\gamma-1}$ , where  $\theta_c$  is the correlation angle [typically  $0.01''$ , Eq. (6.15)] is  $\sim 2 \times 10^{-3}$  in this special case.

Figure 5.—Observability of cosmic backgrounds. Angular scale  $\sigma$  (in radians) is plotted against broad band energy flux,  $F = \nu I_\nu \pi \theta^2 / 4$ , or rms flux variation  $\Delta F$ , in a beam (field of view) of size  $\sigma$ . Uniform cosmic black-body is labeled CBR. A hypothetical "IR" background is shown with  $10^{-2}$  of CBR flux. (At  $100 \mu\text{m}$ , this is roughly the faintest level detectable above zodiacal and galactic emission with coarse angular resolution.) Anisotropy,  $\Delta F$ , is shown for two models of dust clustering: "IRG" with dust distributed in discrete but unclustered galaxies, "IRC" with dust clustered up to a comoving scale  $x_0 \sim 3 \text{ Mpc}$ ,  $\theta_0 \simeq 1.5'$  (cf. § 6.2), and slope  $\beta = 2/5 - \gamma$  in the clustered regime (plotted for  $p = 1$ ,  $\gamma = 2$ ,  $z = 10$ , and  $x_0(t_0) = 10 \text{ Mpc}$ ). The two models are normalized to give similar density contrast on the scale of  $10 \text{ kpc}$ . Confusion limit set by foreground galaxies with assumed properties given in Sec. 7 is shown for diffraction-limited  $100 \mu$  and  $300 \mu$  detectors on a  $1 \text{ m}$  telescope, and for IRAS at  $100 \mu\text{m}$ .

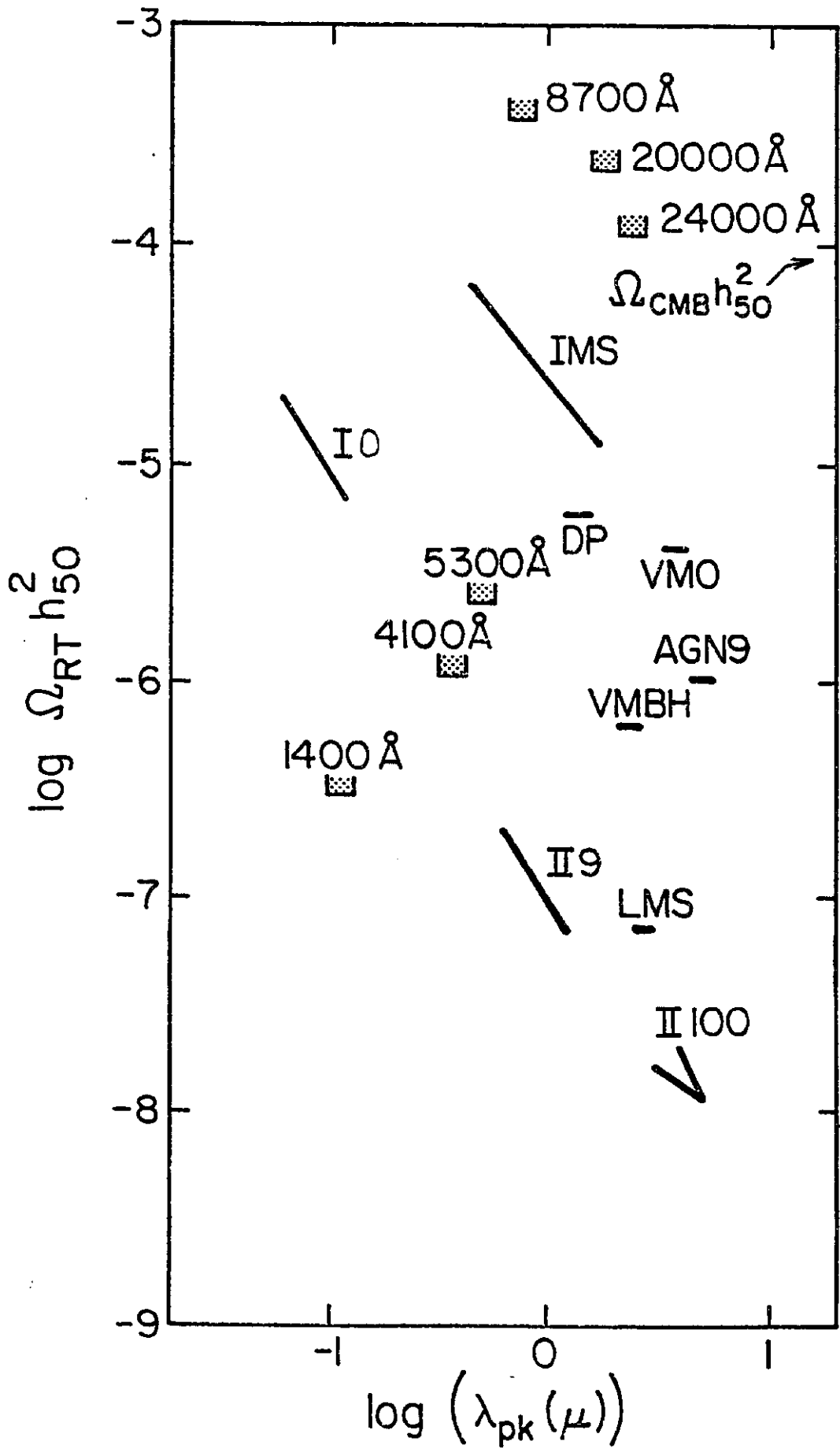


FIG. 1a

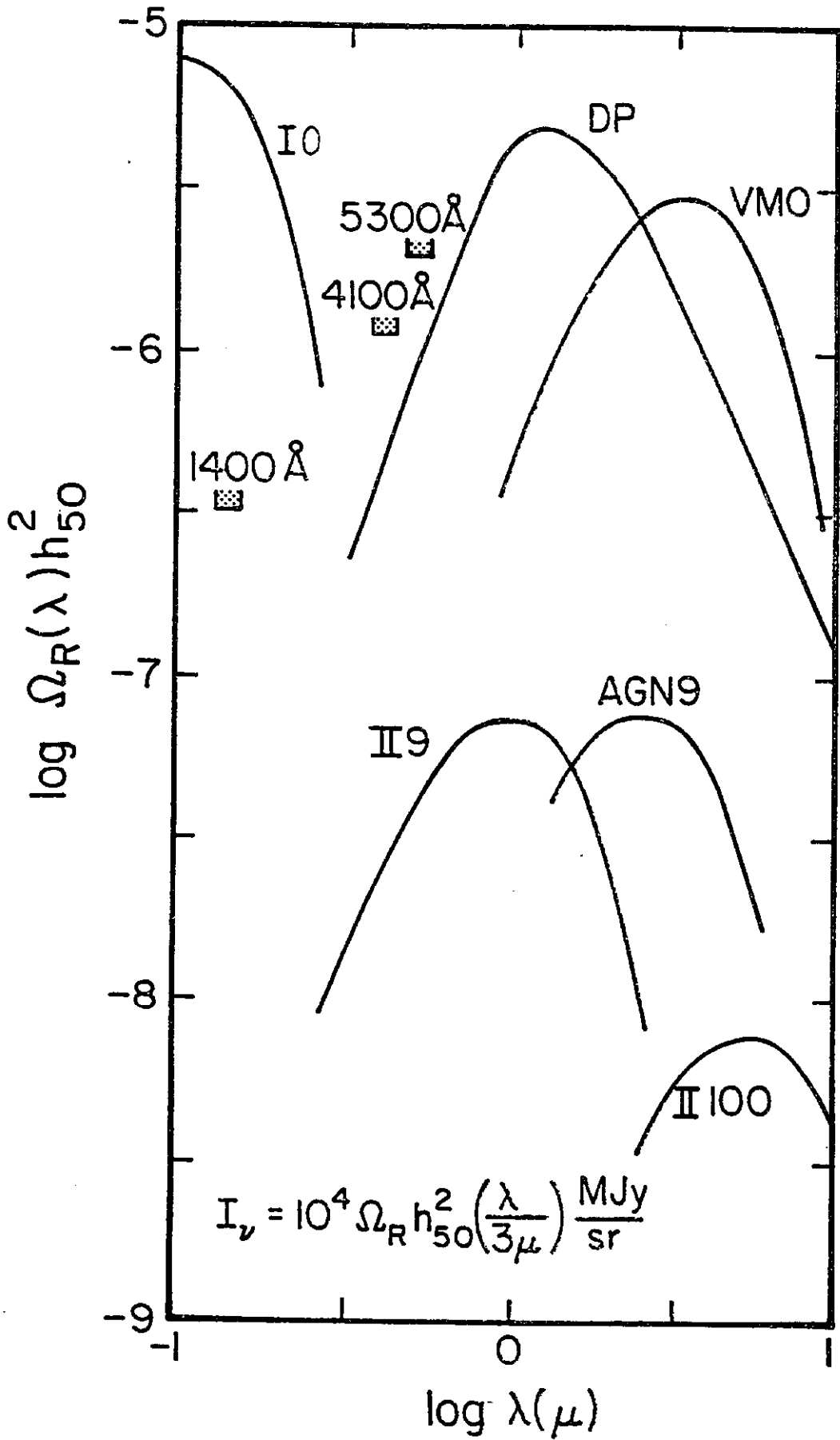


Fig. 1b

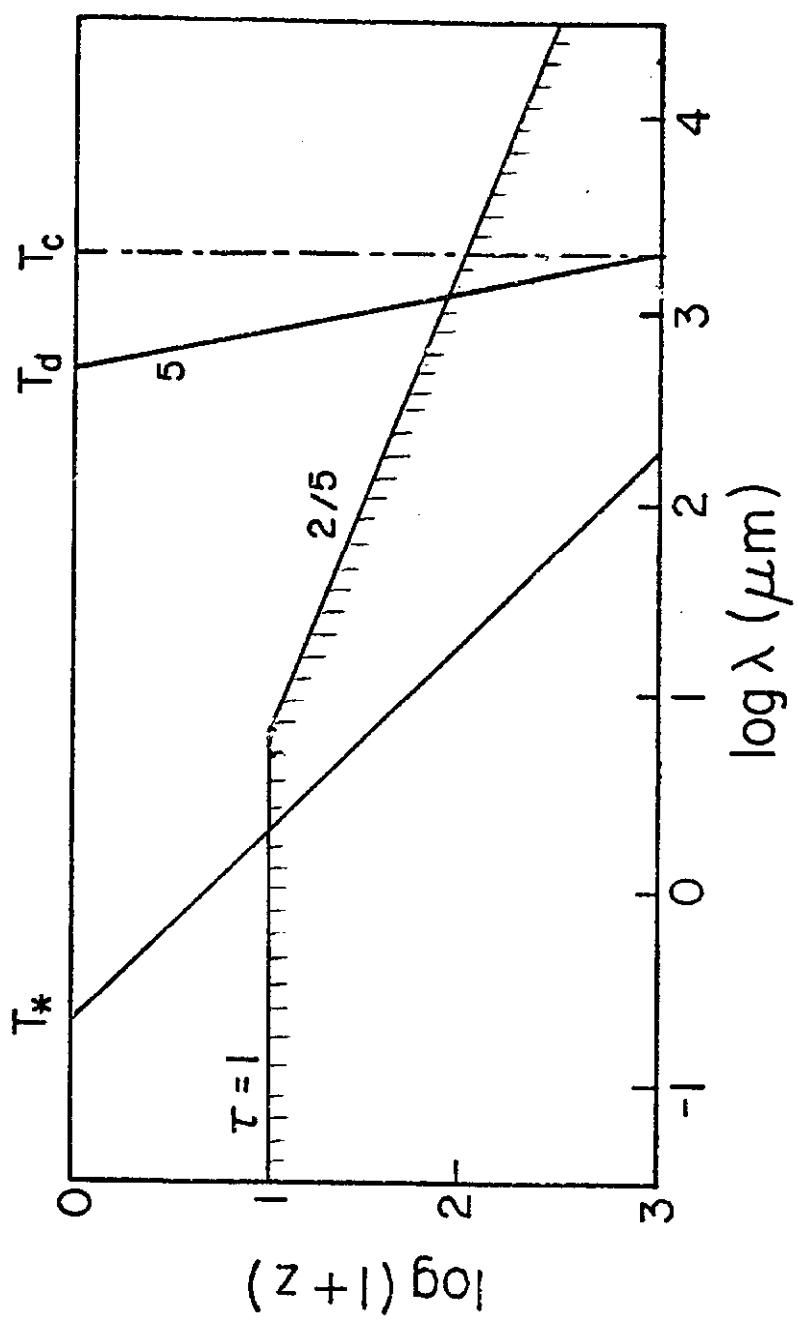


FIG. 2

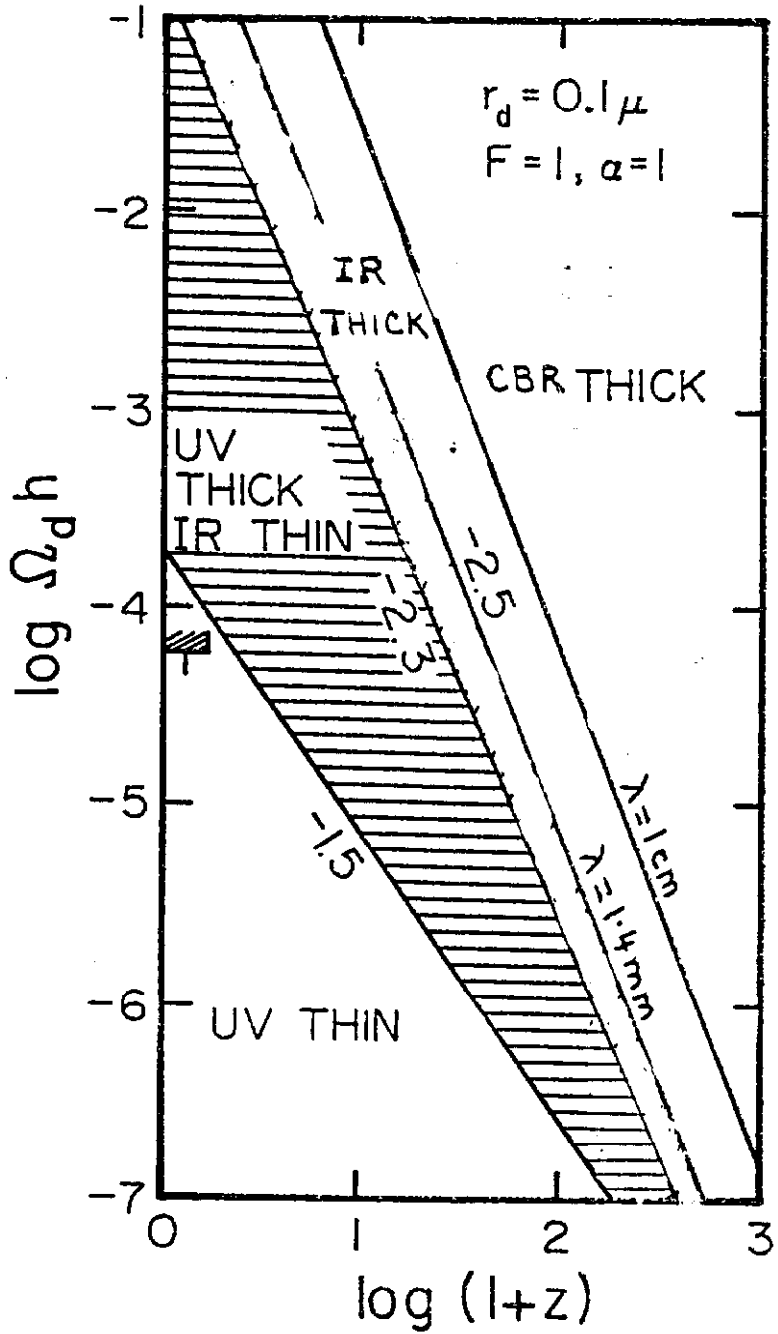


FIG. 3

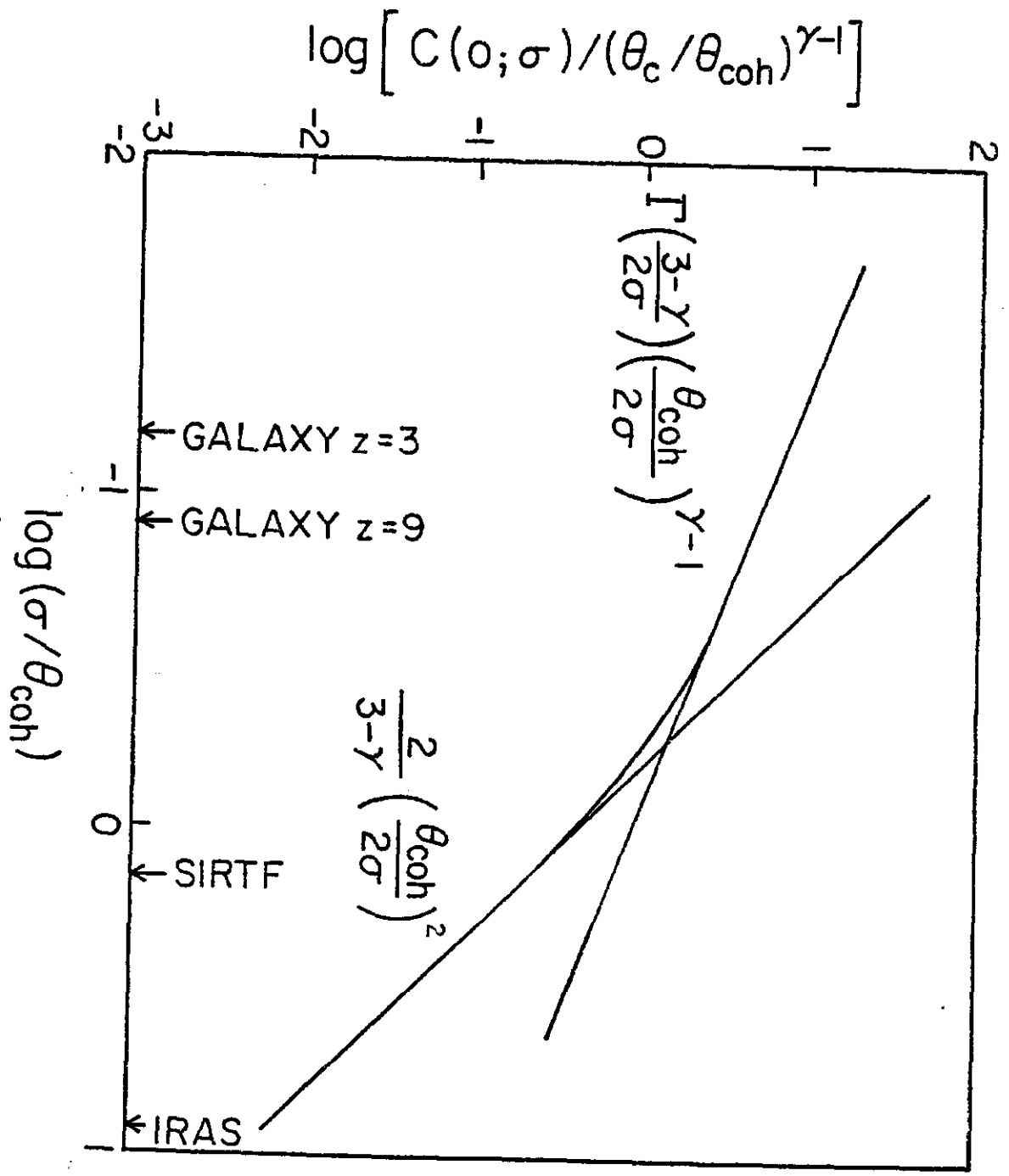


FIG. 4

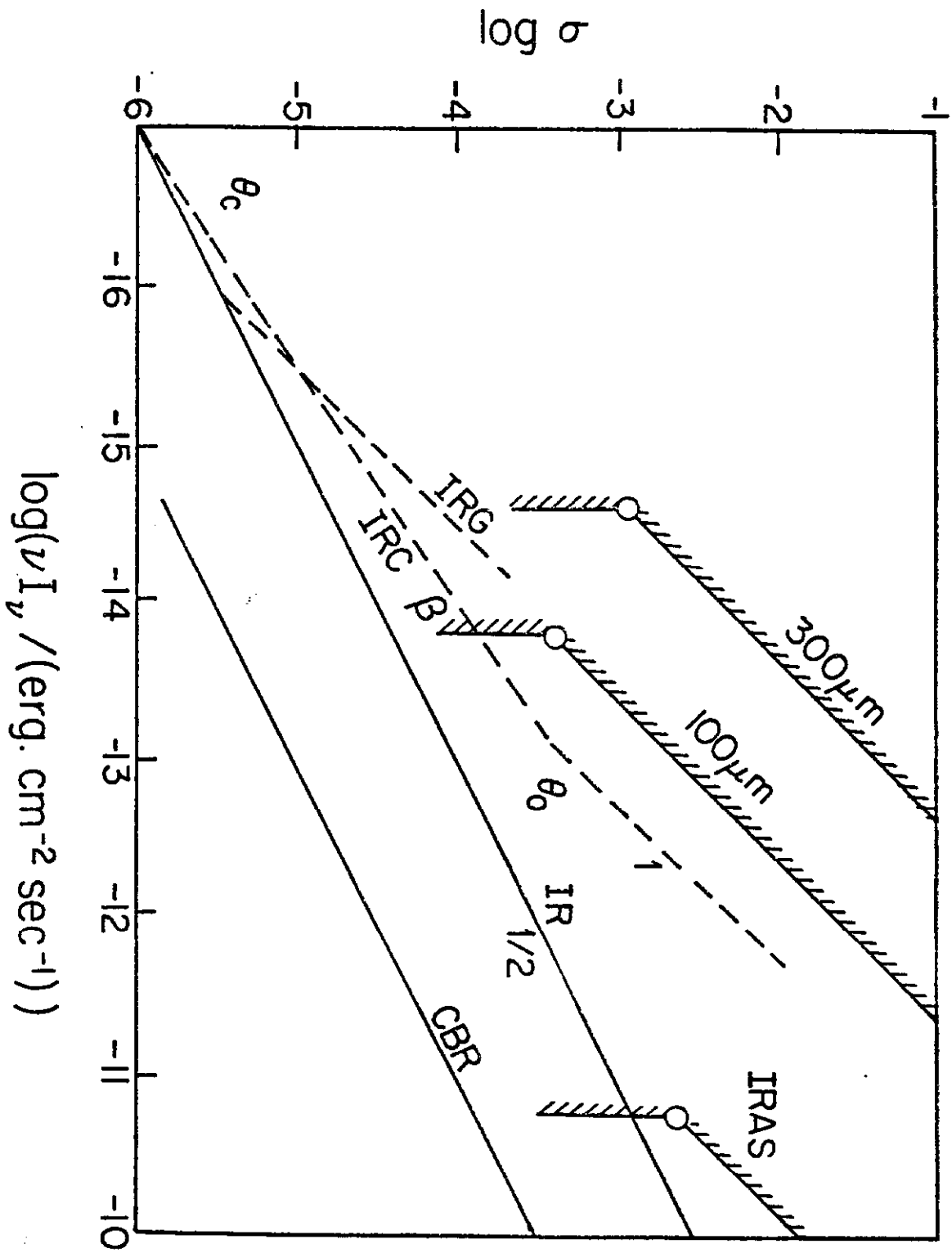


FIG. 5